Geochronological and structural constraints on the Cretaceous thermotectonic evolution of the Kraishte zone, western Bulgaria

Alexandre Kounov,[1] Diane Seward,[2] Jean-Pierre Burg,[2] Daniel Bernoulli,[1,2] Zivko Ivanov,[3] and Robert Handler[4,5]

Received 31 March 2009; revised 18 September 2009; accepted 29 September 2009; published 17 March 2010.

[1] In the Kraishte region, near the junction of the Balkanides and Dinarides, late Early Cretaceous compression led to the thrusting of the Morava unit over the Struma unit. Structural investigations, combined with zircon fission track and $^{40}Ar/^{39}Ar$ analyses, have been used to reconstruct the geological history of the area and to clarify the original tectonic position of the main units before Cenozoic extension. The results show that Early Cretaceous lower amphibolite facies metamorphism and deformation in the Osogovo-Lisets Metamorphic Complex were related to top-to-the-NE directed nappe stacking, whereas the deeper parts of the allochthonous Morava unit experienced low-grade metamorphic overprint at temperatures >~260°C. The structurally intermediate Struma Diorites and their Mesozoic cover experienced temperatures between ~170°C and 300°C. Thrusting of the Morava onto the Struma unit started probably in Valanginian times (140–136 Ma), soon after the cessation of preorogenic to synorogenic turbidite sedimentation on Struma. The metamorphic peak was reached before 112 Ma. Subsequent extension-related cooling of both units was probably accompanied by the formation of low-angle normal faults. **Citation:** Kounov, A., D. Seward, J.-P. Burg, D. Bernoulli, Z. Ivanov, and R. Handler (2010), Geochronological and structural constraints on the Cretaceous thermotectonic evolution of the Kraishte zone, western Bulgaria, *Tectonics*, *29*, TC2002, doi:10.1029/2009TC002509.

1. Introduction

[2] Convergence between Europe and Africa since the Late Cretaceous, together with the independent movement of Adria from the Jurassic to the present, led to the closure of different parts of the Tethys Ocean and the formation of the Alpine-Himalayan orogenic belt [e.g., *Dewey et al.*, 1973; *Dercourt et al.*, 1986; *Ricou et al.*, 1998; *Schmid et al.*, 2008]. This orogenic belt is characterized by along-strike changes of the subduction polarity in central and southeastern Europe, and the formation of two orogenic systems with opposite vergence: the northeast vergent Eastern Alps and Carpathians, and the southwest vergent Dinarides and Hellenides (Figure 1). In the Balkan region, during the Cretaceous–Paleogene, final closure of the Vardar Ocean and of other branches of the oceanic Tethys led to the collision of several distinct tectonic units and the formation of the younger, composite nappe stacks of the Carpatho–Balkan and Dinarides–Hellenic orogenic systems [e.g., *Channell and Horvath*, 1976; *Dercourt et al.*, 1986; *Ricou et al.*, 1998; *Schmid et al.*, 2008].

[3] Whereas palinspastic reconstructions through retro-deformation are relatively straightforward, and the time of deformation can be inferred from unconformities and synorogenic and postorogenic sediments in the external zones of the orogenic system, the internal zones generally defy an easy interpretation. In these internal zones, deep parts of the nappe stack were exhumed by a combination of rock uplift and erosion often connected with extension, and the tectonic relationships in the original nappe stack are not obvious. This is particularly the case in the internal zones of the Carpathian-Balkan-Rhodope segments of the Alpine-Himalayan orogenic belt, where many uncertainties exist about protolith ages and the age of metamorphism and deformation.

[4] The Kraishte is a key location to unravel the Early Cretaceous Alpine-tectonic history of a crucial area in the Carpatho-Balkanic system because Cenozoic extension did not alter some of the Cretaceous structural relationships in the now exposed, metamorphic crustal levels. In this paper, we combine structural observations with new geochronological data based on zircon fission track and $^{40}Ar/^{39}Ar$ analyses for the reconstruction of the Cretaceous orogeny. In particular, we attempt to define the relative position of the major tectonic units of the thrust system before Cenozoic extension and to constrain the age of deformation and metamorphism in the different units.

2. Regional Geology

2.1. Large-Scale Geological Frame

[5] The Balkan mountain chain belongs to the Europe-vergent branch of the Alpine–Mediterranean orogenic belt. It is separated from the Adria-vergent Dinaride–Hellenide system by the oceanic "suture" of the Vardar zone (Figure 1). The external part of the Dinaride–Hellenide system, floored

[1]Institute of Geology and Palaeontology, Basel University, Basel, Switzerland.
[2]Geology Institute, ETH Zurich and Zürich University, Zürich, Switzerland.
[3]Faculty of Geology and Geography, University Kliment Ochridski, Sofia, Bulgaria.
[4]Department for Geography and Geology, University Salzburg, Salzburg, Austria.
[5]Now at Bureau for Geology and Hydrology, Salzburg, Austria.

0278-7407/10/2009TC002509

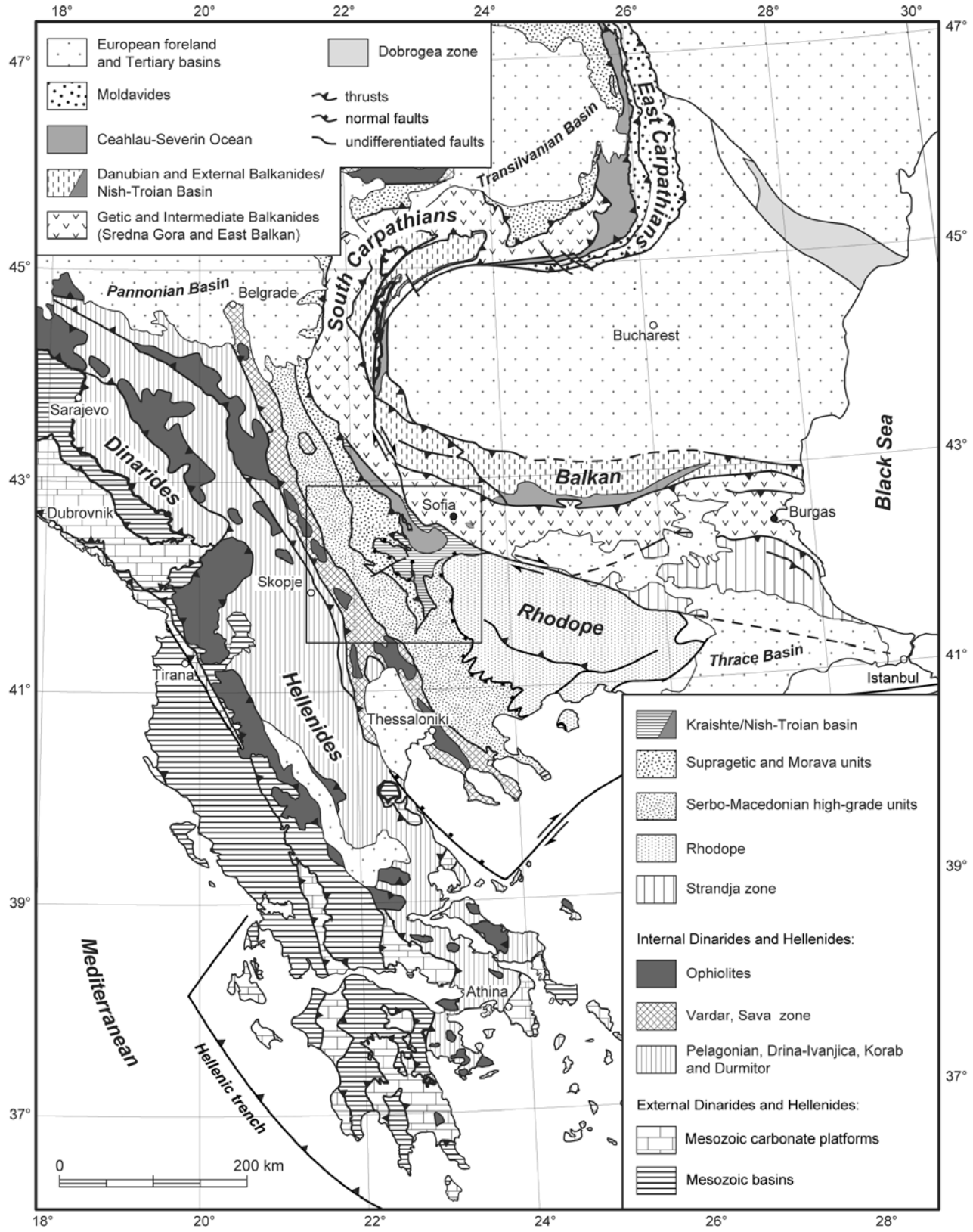

Figure 1. Tectonic map of the southwestern Balkan Peninsula [after *Schmid et al.*, 2008; *Bernoulli*, 2001]. Box outlines Figure 2.

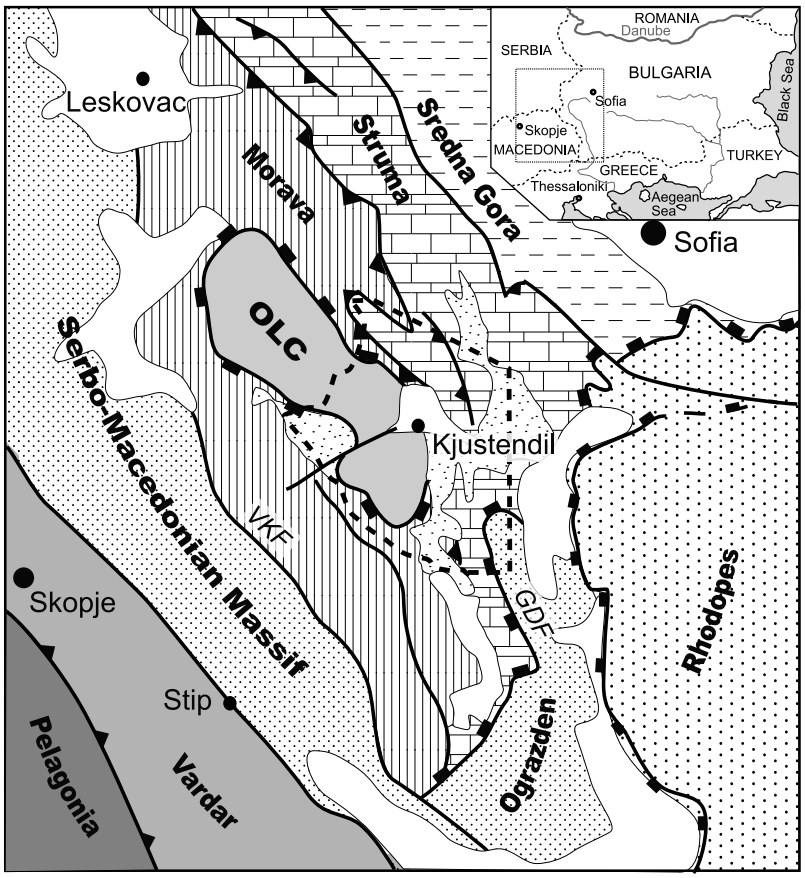

Figure 2. Tectonic overview of the Kraishte area (dashed line for studied area). OLC, Osogovo-Lisets Complex; VKF, Vrvi Kobila fault; GDF, Gabrov Dol Fault. Inset shows geographical location of the map (black area).

by continental crust, was part of a microcontinent or African promontory (Adria), the distal continental margin of which was overthrust in Late Jurassic time by ophiolites derived from the Vardar branch of Tethys. Late Cretaceous, out-of-sequence thrusting led to the formation of composite nappes including Paleozoic rocks occurring in windows below the obducted ophiolites [e.g., *Bernoulli and Laubscher*, 1972; *Zimmerman*, 1972; *Aubouin et al.*, 1976; *Baumgartner*, 1985; *Schmid et al.*, 2008].

[6] In the Carpatho–Balkanic system, possible relics of oceanic rocks are scarce and defectively documented. The external and intermediate zones of the Balkanides (Balkan units, Sredna Gora; Figure 1) have a continental basement and were attached to Europe during Mesozoic times. Deeper marine basins have developed locally (i.e., Nish-Troian Basin, Figure 1), but no ophiolite is known between the Vardar zone and the Moesian platform in the transect of the Balkan–Carpathian junction. In fact, the basement units of the internal western Balkanides can be followed into the crystalline basement nappes of the southern Carpathians [*Kräutner and Kristić*, 2002, available at http://www.geologicacarpathica.sk/special/K/Krautner_Krstic.pdf]. Another major problem is the significance of the so-called "Serbo-Macedonian Massif," a complex area that separates the Balkanides from the Vardar Zone (Figure 1). Originally thought to be an old continental block between two symmetrical orogens ("Zwischengebirge" of *Kober* [1952]), it revealed itself as a complex area composed of metamorphic rocks of different protolith and metamorphic ages.

[7] Our area of research, the Kraishte, is located at the junction between western Bulgaria, east Serbia, and Macedonia (Figures 1 and 2). It is situated between the Late Cretaceous Sredna Gora volcanic arc to the northeast, the Serbo-Macedonian high-grade metamorphic units to the west, and the Rhodopean units to the southeast (Figures 1 and 2). Although juxtaposed during Cenozoic times along crustal-scale extensional fault zones [*Dinter and Royden*, 1993; *Bonev et al.*, 1995], the tectonic units of the Kraishte area and the Serbo-Macedonian Massif on one side and the Rhodopes on the other probably were occupying different crustal levels during their Early Cretaceous tectonic evolution: today, the units of both the Kraishte and Sredna Gora are separated from the high-grade Rhodopean units by a continuation of the low-angle extensional Strymon detachment (Figures 1 and 2) [*Dinter and Royden*, 1993] and from the southeastern extension of the Serbo-Macedonian Massif by

the extensional Gabrov Dol Fault (Figure 2) [*Bonev et al.*, 1995].

[8] In the west, the relationship between the Kraishte unit and the high-grade Serbo-Macedonian units is still debated. The contact has been interpreted as a pre-Mesozoic thrust (Vrvi Kobila fault zone, Figure 2 [*Dimitrijević*, 1997]) or as a post-Late Cretaceous dextral shear zone [*Kräutner and Kristić*, 2002]. Despite the fact that the nature and age of the contact between these two units is still not well defined, they are easily distinguished by the difference in their metamorphic grade.

2.2. Age Constraints for the Balkan Orogeny

[9] Early Cretaceous thrusting is well known from all parts of the Carpatho–Balkan orogenic system [e.g., *Sandulescu*, 1984; *Dimitrijević*, 1997, and references therein]. In the Carpathians, this deformational episode led to the closure of the Ceahlau-Severin Ocean and the imbrication of east facing thrust sheets (Figure 1) [*Sandulescu*, 1984]. The "Austrian" phase began in the late Barremian (circa 130 Ma) as recorded by syntectonic mélanges [*Sandulescu*, 1984]. *Dallmeyer et al.* [1996] reported penetrative Alpine deformation resetting the $^{40}Ar/^{39}Ar$ system between 120 and 100 Ma in the Carpathian. This event is ill-constrained along the link of the southern Carpathian to the Balkans, in Serbia and western Bulgaria, due to the lack of syntectonic sediments and radiometric data [*Dimitrijević*, 1997]. However, ductile overprint of the Sredna Gora basement took place between 106 and 100 Ma in western Bulgaria [*Velichkova et al.*, 2004]. An upper age bracket for Early Cretaceous thrusting and folding in the external Balkan units is set by Santonian (circa 85 Ma) sediments unconformably covering older structures [*Bonchev*, 1986; *Dabovski et al.*, 2002]. In the Rhodope, *Ricou et al.* [1998] suggested pre-Albian stacking of south vergent synmetamorphic nappes including 119–117 Ma high-pressure rocks [*Wawrzenitz and Mposkos*, 1997; *Liati et al.*, 2002].

[10] Late Cretaceous back-arc extension and associated magmatism in the Sredna Gora–Timok–Banat was probably related to the subduction of the Vardar ocean to the northeast [*Boccaletti et al.*, 1974; *Dercourt and Ricou*, 1987; *Burg et al.*, 1996; *Burchfiel et al.*, 2008].

2.3. Kraishte Area

[11] Two major tectonic units can be distinguished in the Kraishte zone (Figure 2): the Morava nappe and the Struma unit. The pre-Alpine evolution of these units needs clarification and their relations to other basement complexes of the area are uncertain; in effect, different parts of these units have been attributed to different tectonic units.

2.3.1. Morava Nappe

[12] The Morava nappe is composed of a continental basement of probable Precambrian-Cambrian age [*Graf*, 2001] with an Ordovician to Devonian sedimentary cover [*Spassov*, 1973; *Zagorchev*, 1984a; *Zagorchev*, 1996]. The basement has undergone greenschist facies metamorphism while the cover experienced only lower grade metamorphic conditions. During the Early Cretaceous the Morava nappe was thrust eastward over the Struma unit [*Dimitrov*, 1931; *Bonchev*, 1936; *Zagorchev and Ruseva*, 1982]. The greenschist facies rocks of the Morava unit were initially thought to be the Paleozoic cover of the crystalline Serbo-Macedonian Massif [*Dimitrijević*, 1967]; only later were they attributed to an independent tectonic unit [*Petrović*, 1969; *Kristić et al.*, 1996; *Zagorchev and Ruseva*, 1982].

[13] The age of thrusting of the Morava unit over the Struma is constrained by the youngest, Tithonian–Valanginian (i.e., circa 150–135 Ma [*Nachev and Nikolov*, 1968]) sediments involved in the thrusting and by the oldest, Late Eocene (i.e., 40–35 Ma), sediments sealing the nappe contact [*Moskovski and Shopov*, 1965]. *Lilov and Zagorchev* [1993] reported 119 Ma as a maximum age for thrusting based on K/Ar whole rock dating of low-grade mylonites in the thrust zone. Several authors, in the Bulgarian literature on the Morava nappe, described at least three thrust sheets with different senses and times of tectonic transport [*Stephanov and Dimitrov*, 1936; *Bonchev*, 1936; *Belmoustakov*, 1948; *Zagorchev and Sapundziev*, 1982]. Somewhat supportively, *Graf* [2001] identified two compression phases during the Cretaceous: (1) D1, top-to-the-SE nappe stacking, and (2) D2, characterized by an average northeastward movement.

2.3.2. Struma Unit and Osogovo-Lisets Complex

[14] The Struma unit consists of variably deformed continent- and ocean-derived rocks with a Vendian–Early Cambrian protolith age (Struma Diorites, 569–544 Ma) [*Stephanov and Dimitrov*, 1936; *Zagorchev and Ruseva*, 1982; *Haydoutov et al.*, 1994; *Graf*, 2001; *Kounov et al.*, 2004], unconformably overlain by a Permian to Lower Cretaceous sedimentary cover [*Zagorchev*, 1980]. The basement also includes the lower amphibolite facies orthogneisses of the Osogovo-Lisets Complex [*Dimitrova*, 1964], which belong to the same magmatic suite as the Struma Diorites, separated from them by a Cenozoic extensional detachment fault system (Figures 2 and 3) [*Graf*, 2001; *Kounov et al.*, 2004]. In the Osogovo-Lisets Metamorphic Complex, the original underpinnings of the Struma unit, *Zagorchev* [2001] described several generations of folds and foliations and at least three metamorphic events. According to this author, the main metamorphic event took place under amphibolite facies conditions during the Vendian–Early Cambrian, whereas the Variscan and the Alpine overprints were restricted to the formation of large anticlines and low-grade shear zones; however, these attributions were not supported by geochronological data. *Zagorchev* [1995, 2001] speculated that the Morava unit had been thrust directly onto the deeply eroded Osogovo-Lisets antiform exposing crystalline basement rocks in its core and Mesozoic nonmetamorphosed sediments on its flanks.

[15] By contrast, later studies in the Kraishte area have shown contacts previously interpreted as thrust faults to be low-angle normal faults and thus established that extensional faults accompanying exhumation have cut out part of the older tectonic structure of the Osogovo-Lisets dome [*Graf*, 2001; *Kounov et al.*, 2004].

2.3.3. Cenozoic Extension

[16] During the middle Eocene to Oligocene extensional phase (circa 40–30 Ma), basins were formed and were filled with continental and marine deposits (Figure 3). Both, the sediments and their basement, were intruded by rhyolitic to

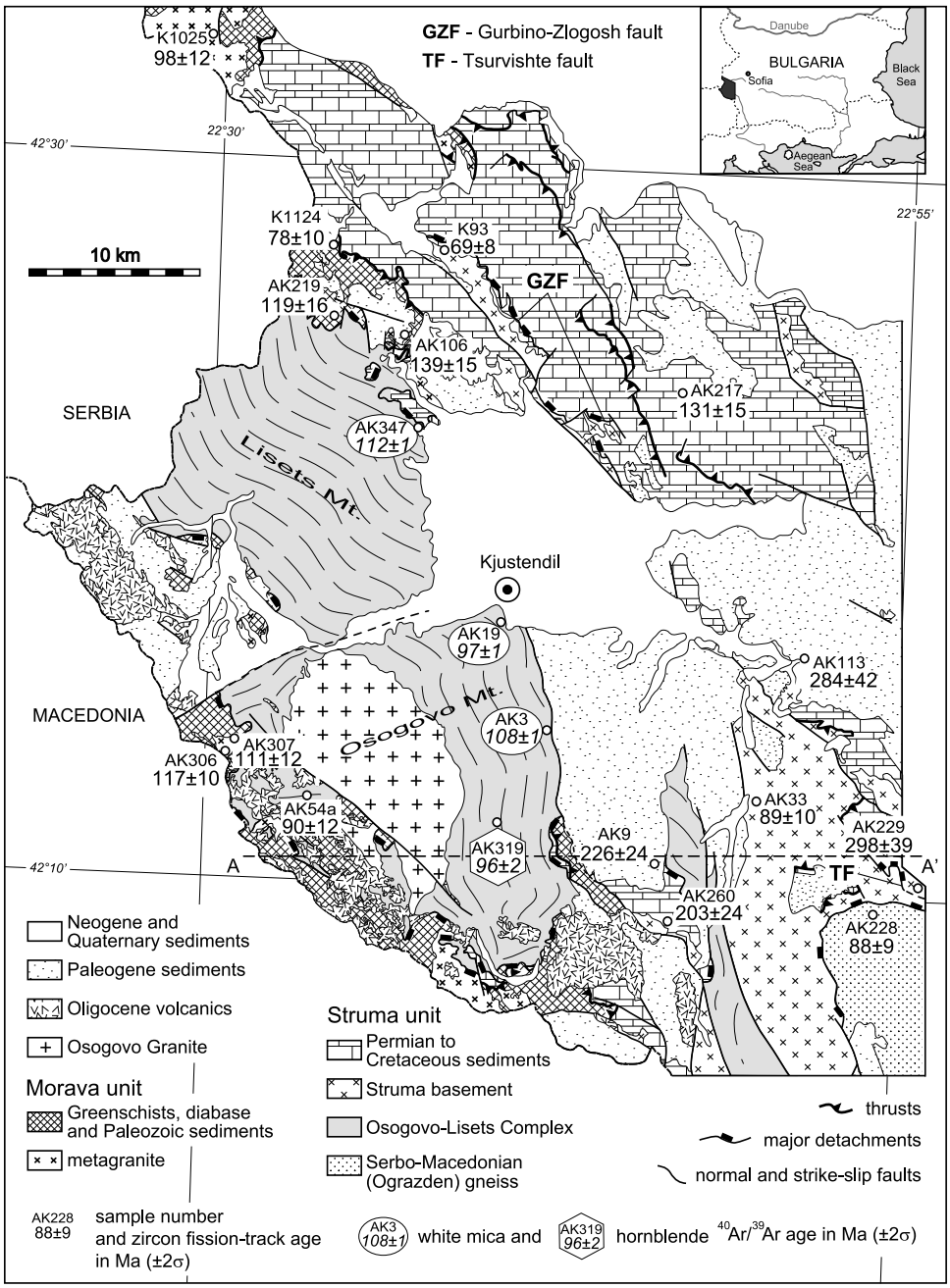

Figure 3. Geological map of the Kraishte area (SW Bulgaria) modified from *Moskovski* [1968], *Zagorchev and Ruseva* [1993], and *Zagorchev* [1993] with location and ages of analyzed samples. Inset shows geographical location of the map (black area). Line AA′ is the section in Figure 11.

dacitic subvolcanic bodies and dikes at circa 32–29 Ma [*Harkovska and Pecskay*, 1997; *Kounov et al.*, 2004] and by the 31 ± 2 Ma Osogovo Granite [*Graf*, 2001].

[17] Cenozoic extension probably was also responsible for the exhumation of part of the Serbo-Macedonian Massif in the southeast of the study area in the so-called Ograzden unit in Bulgaria [*Zagorchev*, 1984b], which correlates with the Lower Serbo-Macedonian Massif in Serbia [*Dimitrijević*, 1967]. The unit consists of amphibolite facies metamorphic rocks and is separated from the overlying Struma Diorites by the Gabrov Dol detachment [*Bonev et al.*, 1995].

3. Analytical Methods

[18] The combination of zircon fission track (FT) and $^{40}Ar/^{39}Ar$ analyses is a powerful approach to document the thermal and exhumation history of rocks in the temperature interval of ~500–170°C [*McDougall and Harrison*, 1999;

Tagami, 2005]. The geographical location of the samples and the results are presented in Figure 3 and Table 1, and the analytical procedures are described in Appendix A.

[19] The temperature at which fission tracks in zircon anneal is not sharply defined. A temperature range exists where partial track annealing occurs (partial annealing zone, PAZ). Wide-ranging values for the temperature bounds of partial FT annealing within zircon have been published, and following common diffusion behavior, it is accepted that at high cooling rates the closure of the radiometric system takes place at higher temperatures. The latest estimations of the zircon partial annealing zone based on short-term laboratory experiments (10^{-1}–10^{4} h) and extrapolated to geological timescales (10^{6} years) suggest a wide range of temperature limits, varying between ~390°C and 170°C [e.g., *Yamada et al.*, 1995; *Tagami and Dumitru*, 1996; *Tagami et al.*, 1998; *Tagami*, 2005]. Long-term annealing characteristics of fission tracks in zircon have been studied in samples from deep boreholes [*Zaun and Wagner*, 1985; *Coyle and Wagner*, 1998; *Green et al.*, 1996; *Tagami et al.*, 1996; *Hasebe et al.*, 2003]. These analyses show that fission tracks were stable (no annealing) up to temperatures of ~200°C, and the total annealing temperature is higher than ~320°C. Following the results of these studies here we assume an effective closure temperature for zircon of 260°C ± 50°C.

4. Results

4.1. Structural Observations

4.1.1. Osogovo-Lisets Metamorphic Complex

[20] Our structural investigations focused on the Osogovo-Lisets dome (Figure 4). This metamorphic and magmatic dome consists mainly of granitic, dioritic to gabbroic rocks intruded by leucocratic granites, all highly deformed and transformed to muscovite and two-mica gneisses and amphibolites. The main foliation S_1 is defined by flattened quartz – feldspar aggregates and growth of new white mica and biotite which is often altered to white mica and chlorite. S_1 generally dips 20° to 65° toward the NE and becomes steeper near the contact with the Osogovo Granite (Figures 4 and 5). The stretching lineation, on S_1, typically plunges NE to NNW with the exception of the southeastern slope of Osogovo Mountain where a SSW direction was measured along the south to SW dipping foliation planes (Figure 4). These structural features define a dome formed most probably by tilting during the Cenozoic extension and emplacement of the undeformed Oligocene (32 Ma) Osogovo Granite (Figure 4) [*Kounov et al.*, 2004]. In general, the contact of the Osogovo Granite follows more or less the S_1.

[21] Compared to the Osogovo Mountain, the main foliation S_1 in the Lisets Mountain dips 5° to 55° consistently toward the NE and bears a lineation plunging to the NE (Figure 4). Usually, the dominant direction of fold axes in the Osogovo-Lisets gneisses trends SW–NE to SSE–NNW and coincides with the orientation of the stretching lineation (Figure 4). However, in less deformed areas, especially in the northern slope of Lisets Mountain, east to SE and WNW plunging fold axes are present (Figure 4).

[22] There is a general decrease of the deformation intensity and, probably, temperature conditions from the Osogovo Mountain toward the northern part of Lisets Mountain where deformation appears to be less penetrative and often localized along shear zones (Figures 4 and 5). In some places, on the northeastern slope of the Lisets Mountain, undeformed zones displaying primary magmatic structures are preserved (Figure 6a). In the high-strain mylonites, common in the Osogovo Mountain, recrystallized elongate ribbons of quartz and stretched feldspar aggregates are present (Figure 6b), whereas in the less deformed rocks from the northern part of Lisets Mountain, core and mantle structures and microkinking of feldspar are more prominent (Figure 6c). There is no sharp boundary between these two domains (Figure 5) but the rocks of Osogovo may have been deformed at somewhat deeper levels. Indeed, the gneisses of the Osogovo Mountain and the southern slope of the Lisets Mountain have been deformed under higher temperature, perhaps also at deeper levels. The gneisses from these areas have experienced a greater amount of exhumation/denudation during Cenozoic extension due to the southwestward movement on the main Eleshnitsa detachment (Figures 4 and 5) [*Kounov et al.*, 2004]. Later exhumation of the Osogovo Mountain and warping of the Eleshnitsa detachment might be due to the emplacement of the Osogovo Granite. The mylonitic shear zones are very difficult to follow laterally because of the discontinuous outcrops and the intense, Cenozoic brittle overprint.

[23] Throughout the Osogovo-Lisets Complex, macrocriteria and microcriteria for the sense of shear show dominantly north to northeastward tectonic transport. Kinematic indicators such as shear bands and asymmetric clasts are common (Figure 6d). Other shear sense indicators such as "mica fish" and quartz grains recrystallized obliquely to the mylonitic foliation were observed in oriented thin sections (Figures 6e and 6f).

[24] In many places of the Osogovo-Lisets dome, a retrogressive metamorphic overprint was mostly restricted to discrete fault zones (Figures 4 and 5). This overprint is associated with the formation of extensional crenulation cleavage, cohesive breccias and gouges. This type of deformation mostly affected the highest structural levels near the detachments and is related to Cenozoic extension (Figures 4 and 5) [*Kounov et al.*, 2004].

4.1.2. Morava and Struma Units

[25] Detailed structural investigations in the Morava and Struma units were beyond the scope of this study. Nevertheless, lower metamorphic-grade structures were observed in the Morava greenschists in the southwestern slope of Osogovo Mountain as well as in the Struma unit. In the Morava unit, northeastward tectonic transport direction as in the Osogovo-Lisets metamorphics was measured (Figure 7).

[26] In the Struma Diorites, ductile deformation is localized in discrete shear zones. Unfortunately, the thrust contact in the northern part of the studied area, where the Morava unit directly lays over the Mesozoic sediments of the Struma unit, is often covered and has been reactivated during Cenozoic extension as low-angle fault. Where observed, this contact is

Table 1. Fission Track Analysis on Zircons[a]

Sample	Grid References	Altitude (m)	Lithology	Number of Grains	ρ_d (Nd) ($\times 10^6$ cm^{-2})	ρ_s (Ns) ($\times 10^6$ cm^{-2})	ρ_i (Ni) ($\times 10^6$ cm^{-2})	P(χ^2) (%)	Variation (%)	U Concentration (ppm)	Central Age ± 2σ (Ma)
					Morava Unit						
K1025	N42.57330/E022.48878	1060	granite	20	0.4087(2747)	17.34(1607)	4.727(438)	54	7	451	98.4 ± 11.8
K1124	N42.46169/E022.56913	825	diabase	16	0.4030(2747)	8.759(1101)	2.983(375)	95	0	289	77.7 ± 9.8
AK219	N42.41828/E022.57276	640	sandstone	18	0.2899(2093)	13.64(1675)	2.179(267.6)	99	0	301	118.7 ± 16.4
AK306	N42.20429/E022.50826	1851	granite	20	0.3970(2761)	10.86(3431)	2.418(764)	90	0	238	116.6 ± 10.4
AK307	N42.21171/E022.52372	1698	granite	18	0.3883(2761)	14.51(2110)	3.322(483)	98	0	334	111.0 ± 12.0
AK106	N42.42128/E022.62260	900	granite	18	0.3754(2761)	9.524(2662)	1.685(471)	84	<1	175	138.5 ± 14.8
					Struma Unit: Basement						
K93	N42.46148/E022.65220	922	orthogneiss	14	0.4201(2747)	15.09(1253)	6.022(500)	99	0	559	69.1 ± 7.8
AK33	N42.17604/E022.57912	550	granite	26	0.4011(2721)	11.40(2050)	3.365(605.3)	12	15	327	89 ± 10.4
AK54a	N42.17468/E022.56020	2030	metadiorite	22	0.4400(2722)	9.157(1049	2.933(336)	98	0	260	90.0 ± 11.8
AK113	N42.24827/E022.89954	445	granite	20	0.3687(2093)	22.37(2658)	1.873(222.5)	97	0	198	284.3 ± 41.6
AK229	N42.12651/E022.99138	480	diorite	20	0.3868(2093)	20.60(3579)	1.727(300)	63	6	174	297.8 ± 39.0
					Struma Unit: Sedimentary Cover						
AK217	N42.37055/E022.81052	1005	sandstone	27	0.3503(2093)	20.84(3357)	3.610(581.4)	14	14	402	131 ± 15.0
AK260	N42.11145/E022.80584	951	sandstone	21	0.4185(2761)	27.20(2825)	3.636(377.6)	95	0	339	203.4 ± 23.6
AK9	N42.14067/E022.80550	710	sandstone	22	0.4890(2651)	28.06(3452)	3.935(484)	99	0	314	226.2 ± 23.6
					Ograzden Unit						
AK228	N42.11968/E022.95317	730	orthogneiss	20	0.3626(2093)	19.19(2479)	5.203(672)	91	0	560	87.7 ± 8.6

[a]The parameters ρ_d, ρ_s, and ρ_i represent the standard, sample spontaneous, and induced track densities, respectively. Nd, Ns, and Ni are the number of tracks counted. P(χ^2) is the probability of obtaining χ^2 values for ν degrees of freedom, where ν is the number of crystals −1. All ages are central ages [*Galbraith*, 1981]. $\lambda D = 1.55125 \times 10^{-10}$. A geometry factor of 0.5 was used. Zeta = 132 ± 3 for CN1/zircon. Irradiations were performed at the ANSTRO facility, Lucas Heights, Australia.

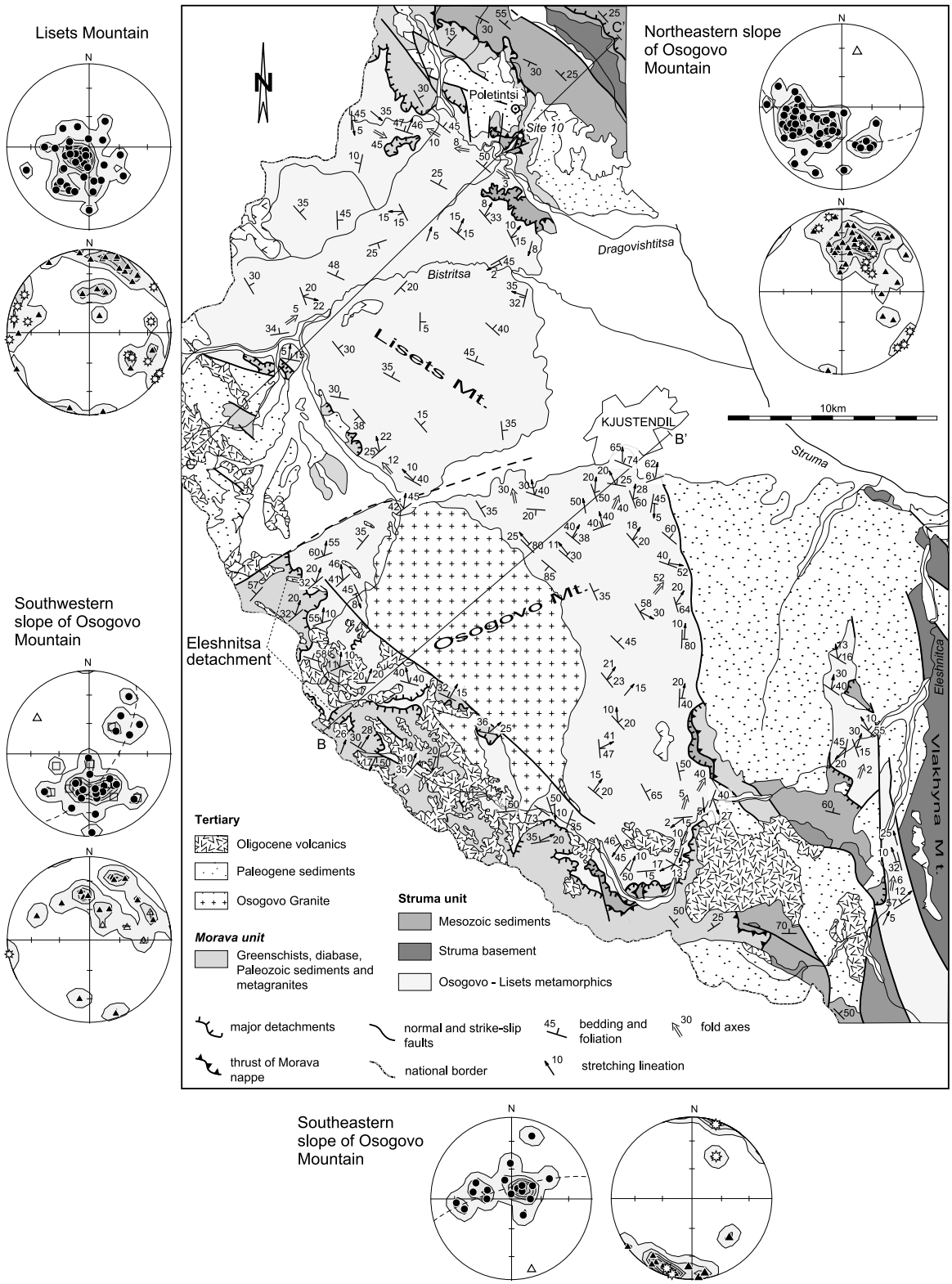

Figure 4. Geological map of the Kraishte area (Figure 3) with lower hemisphere equal-area plots of structural elements. Solid circles indicate foliation poles from Osogovo-Lisets Complex; open squares indicate foliation poles from Morava unit; closed triangle indicate stretching lineation from Osogovo-Lisets Complex; open triangles indicate stretching lineation from Morava unit; asterisks indicate fold axes; big open triangle indicate best fit great circle of the foliation. Lines BB′ and CC′ are the sections in Figure 5.

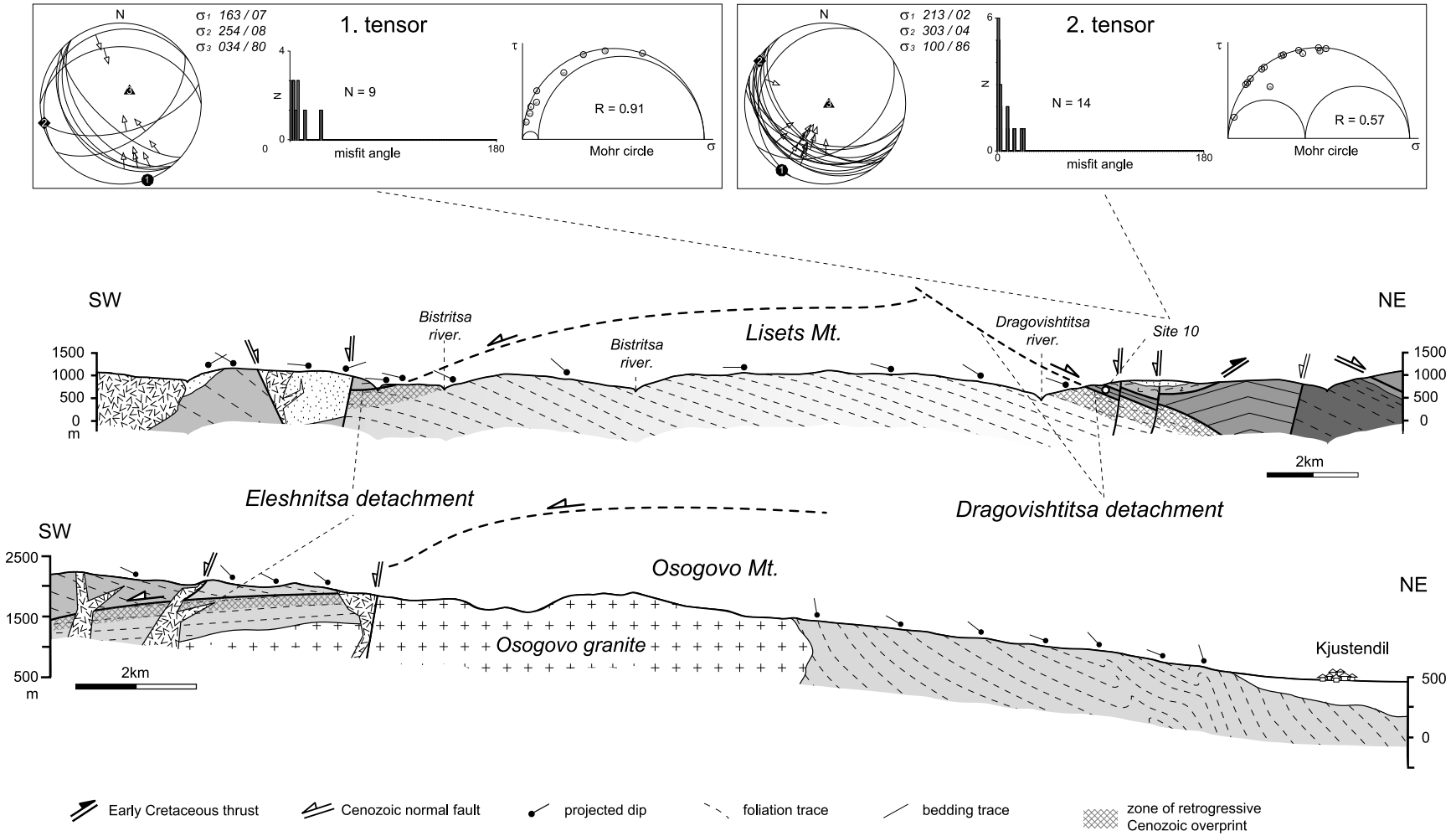

Figure 5. Cross sections through the Osogovo and Lisets mountains with lower hemisphere, equal-area plots of brittle fault slip striations measured in Middle Triassic limestones near Poletintsi (site 10, Figure 4). Maximum, intermediate, and minimum stress axis (σ_1, σ_2, and σ_3) are presented as closed circle, rhombs, and triangles, respectively. Distribution of the misfit angle is given in the histogram (N, number of faults; x axis, misfit angle) and the stress tensor aspect ratio R is represented in a Mohr circle diagram (τ, shear stress; σ, normal stress). Paleostress data processing was carried out using Software FSA written by B. Célérier, which is based on a direct inversion algorithm [*Bott*, 1959; *Compton*, 1966; *Etchecopar et al.*, 1981]. For location, see Figure 4 traces BB′ and CC′. Lithological key is as in Figure 4.

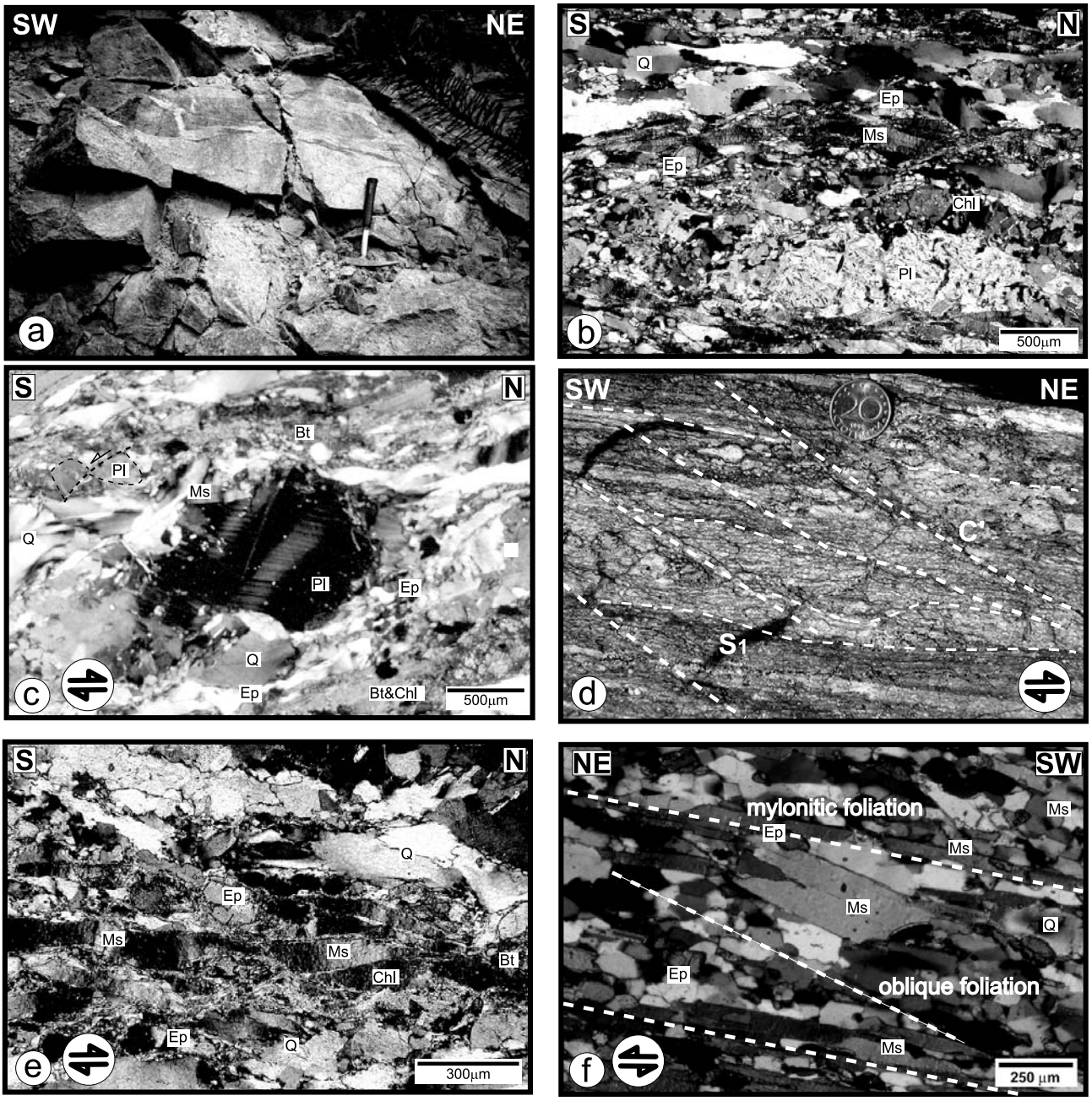

Figure 6. Structural features of the Osogovo-Lisets Complex. (a) Compositional layering in gabbro, northeastern slope of Lisets Mountain. (b) Recrystallized elongate ribbons of quartz and stretched feldspar aggregates, southeastern slope of Osogovo Mountain. (c) Plagioclase porphyroclast showing kinking. In the upper left corner, antithetic microfaulting of small plagioclase crystal. Top-to-the-north sense of shear, southeastern slope of Osogovo Mountain. (d) C′ shear bands indicating top-to-the-NE sense of shear, Osogovo-Lisets metamorphics north of Kjustendil. (e) Mica fish showing top-to-the-north sense of shear (biotite is often replaced by chlorite), southeastern slope of Osogovo Mountain. (f) Oblique and mylonitic foliation in the gneisses from the southeastern slope of Osogovo Mountain. Sense of movement is top-to-the-NE. The coarse white mica in the middle crystallized before that on the mylonitic foliation planes. Abbreviations are Q, quartz; Ep, epidote; Ms, muscovite; Chl, chlorite; Pl, plagioclase; Bt, biotite.

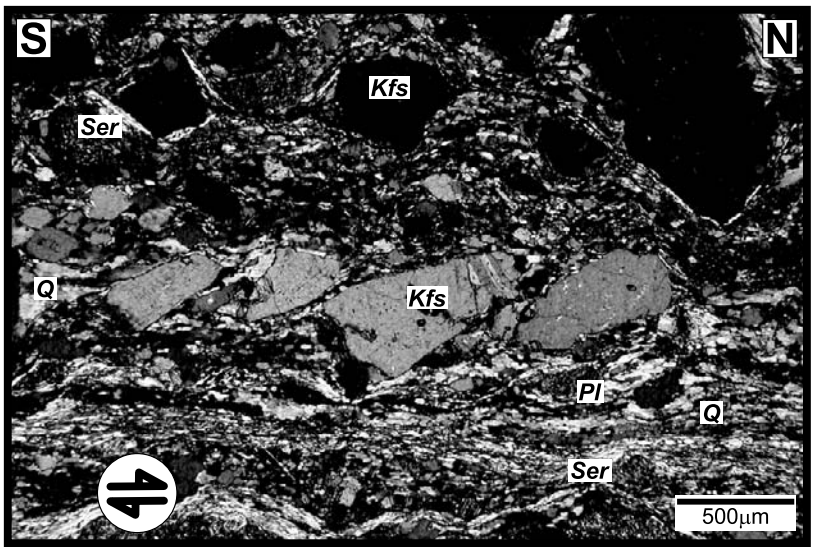

Figure 7. "Bookshelf" microfracturing of feldspar crystal showing top-to-the-north sense of shear in Morava schists, southwestern slope of Osogovo Mountain. Abbreviations are Kfs, K-feldspar; Ser, sericite; Q, quartz; Pl, plagioclase.

dominantly brittle. The best exposure is situated south of the village of Poletintsi (Figures 4 and 5). Here the paleostress calculation (using Software FSA written by B. Célérier) derived from fault slip measurements in Middle Triassic limestones reveals two stress tensors, which we relate to the Cretaceous compressions (Figure 5). The first tensor integrates dominantly SW to SE dipping thrust faults. The maximum compressive σ_1 axis is horizontal and trends SSE–NNW (Figure 5). The second tensor stems from mostly SW dipping thrust faults with SW plunging striations. The compressive σ_1 axis is subhorizontal and trends SSW–NNE. *Graf* [2001] reported similar tensor orientations related to thrusting of Morava onto the Struma unit in the Kraishte area. Our data are too scarce for general conclusions but the first tensor fits the D1 deformation stage of *Graf* [2001] whereas the second tensor matches his D2 stage.

4.2. Thermochronology

4.2.1. The $^{40}Ar/^{39}Ar$ Data

[27] Four samples (three white micas and one hornblende) were analyzed from various rocks of the Osogovo-Lisets Metamorphic Complex. In addition, the white mica and the biotite of the AK228 muscovite-biotite gneiss of the Ograzden unit (Figure 3) were analyzed. In the tables of analytical data (Table A1) $^{37}Ar/^{39}Ar$ ratios do not show a correlation with the apparent ages, and therefore, $^{37}Ar/^{39}Ar$ versus cumulative ^{39}Ar plots are not included in Figure 3. For most of the samples inverse isochron plots yielded mixtures of atmospheric and radiogenic Ar components, indicated by $^{40}Ar/^{36}Ar$ intercepts close to atmospheric composition. Exceptions are the white micas from samples AK3 and AK347 whose Ar is almost entirely radiogenic. The inverse isochron plot for muscovite sample AK228 suggests the presence of inherited excess ^{40}Ar, which is also recognized in the disturbed age patterns.

[28] MSWD values calculated for isotope correlation are too high (>2.5), which may indicate that a linear relation between the data in the inverse isochron plots may not exist.

4.2.1.1. Osogovo-Lisets Metamorphic Complex

[29] Step heating of a white mica sample from a deformed aplitic vein (sample AK3, Figure 2) in the eastern Osogovo-Lisets Complex, near the contact with Paleogene sediments (Figure 3), yields a reliable 108 ± 1 Ma plateau age (Figure 8). The high $^{37}Ar/^{39}Ar$ ratios in the low- to medium-temperature increments of the experiment (Table A1) are likely due to the presence of two mineral phases with a different Ca content, but of the same age. The first phase may correspond to the white mica from the aplitic vein, whereas the second may be the mica on the foliation plane, related to the lower amphibolite facies deformation. Further north, near Kjustendil, the white mica from a deformed leucogranite AK19 (Figure 3) has a perfect age spectrum revealing a plateau at 97 ± 1 Ma (Figure 8). Sample AK347, a granitic gneiss from the eastern slope of Lisets Mountain, near the Cenozoic detachment (Figure 3), also has an almost undisturbed white mica age spectrum, with a reliable plateau age of 112 ± 1 Ma (Figure 8).

[30] Hornblende from the amphibolite sample (AK319) collected in the Osogovo gneisses approximately 3 km east of the contact with the Osogovo Granite (Figure 3) shows no disturbances in the $^{37}Ar/^{39}Ar$ ratio and age spectra, yielding a plateau age of 96 ± 2 Ma (Figure 8).

4.2.1.2. Ograzden Unit

[31] Both white mica and biotite from sample AK228, collected near the contact with the Struma Diorites (Figure 3), were analyzed. It was not possible to calculate a plateau age for the muscovite, due to presence of excess ^{40}Ar (Figure 8). Nevertheless the last 6 high-temperature gas-release steps yielded ages at ~160 Ma. The biotite shows no correlation between $^{37}Ar/^{39}Ar$ and the age spectrum. The staircase-type pattern indicates initial isotopic closure at ~80 Ma, followed

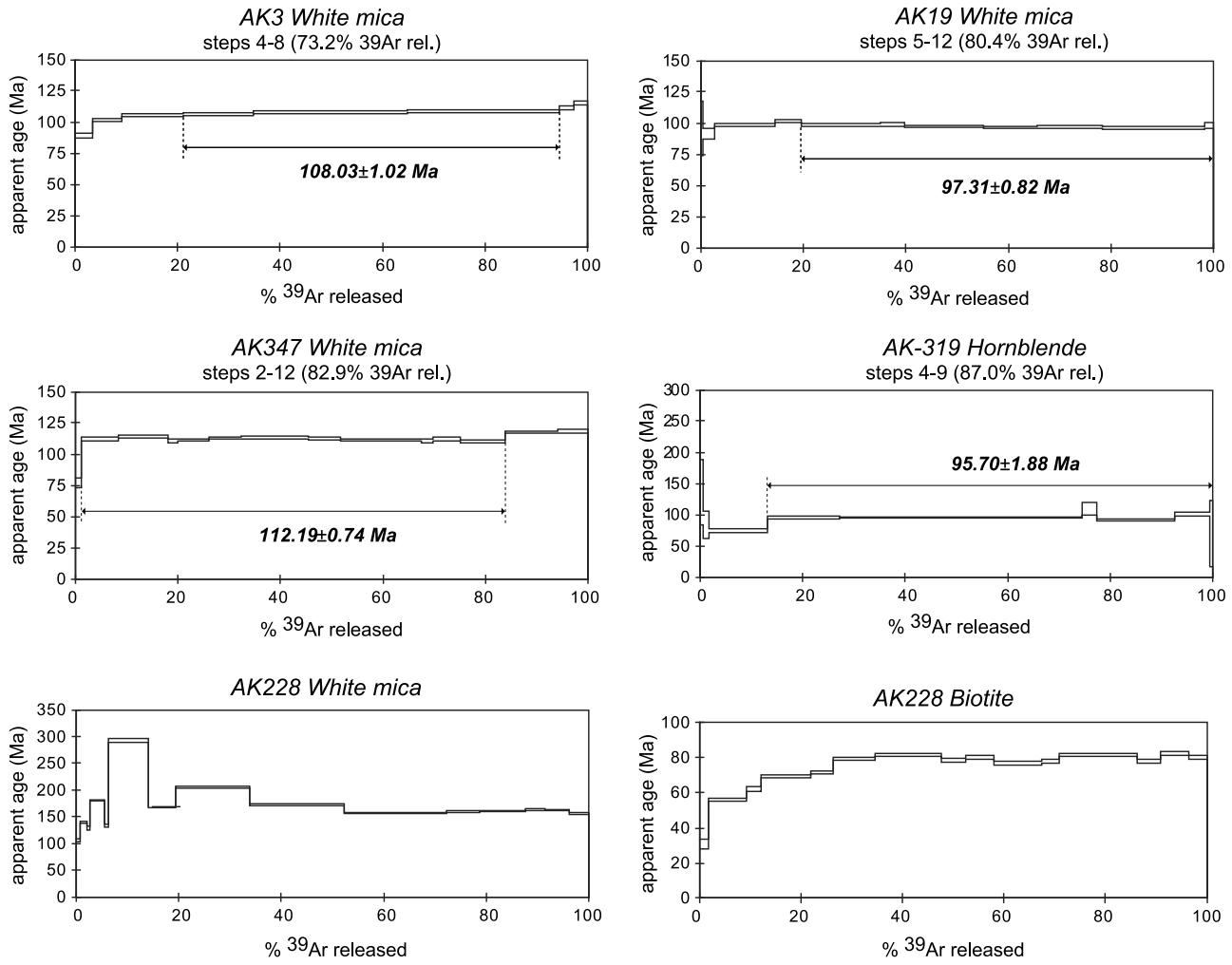

Figure 8. The $^{40}Ar/^{39}Ar$ age spectrum diagrams for samples from the Osogovo-Lisets metamorphics and Ograzden gneisses. Steps used for calculation of plateau ages are indicated by arrows.

by partial resetting probably due to a later thermal event at ~30 Ma (Figure 8 and further discussion).

4.2.2. Fission Track Data

4.2.2.1. Morava Unit

[32] All zircon samples from the Morava unit yielded Cretaceous fission track (FT) ages between 119 ± 16 and 78 ± 10 Ma (Table 1). The only exception concerns a ~30 cm in diameter, undeformed granite boulder (sample AK106) collected from a Paleogene alluvial fan breccia (Figure 3), which yielded an age of 139 ± 15 Ma. The probability that this boulder underwent relatively little transport, and the fact that the contact to Morava granites is only a few hundred meters away supports the idea that it is derived from this unit.

4.2.2.2. Basement of the Struma and Ograzden Units

[33] Three deformed samples from the Struma Diorites (K93, AK54a and AK33, Figure 3) yielded Cretaceous zircon FT ages of 69 ± 8, 90 ± 12 and 89 ± 10 Ma, respectively. In the eastern part of the study area (Figure 3), two undeformed diorite samples (AK113 and AK229) yielded much older zircon FT ages of 284 ± 42 and 298 ± 39 Ma, respectively.

[34] The two-mica gneiss from the Ograzden unit (AK228, Figure 3) yielded a zircon FT age of 88 ± 9 Ma, close to the initial isotopic $^{40}Ar/^{39}Ar$ closure age (~80 Ma) obtained from biotite of the same sample.

4.2.2.3. Mesozoic Sediments of the Struma Unit

[35] The Lower Triassic sandstone (AK260, Figure 3) yielded a zircon FT age of 203 ± 24 Ma. A sandstone clast (AK9, Figure 3), collected from the basal breccia of the Paleogene sedimentary series and probably derived from the nearby outcropping Lower Triassic sandstones, yielded an age of 226 ± 24 Ma. A sandstone sample from Tithonian–Valanginian turbidites (AK217) has a zircon FT age of 131 ± 15 Ma. Although all three samples pass the χ^2 test (higher than 5%), they do show a relatively large spread of single grain ages (Figure 9).

5. Interpretation and Discussion

[36] Based on the thermochronological and structural data we can now discuss the position of the different tectonic

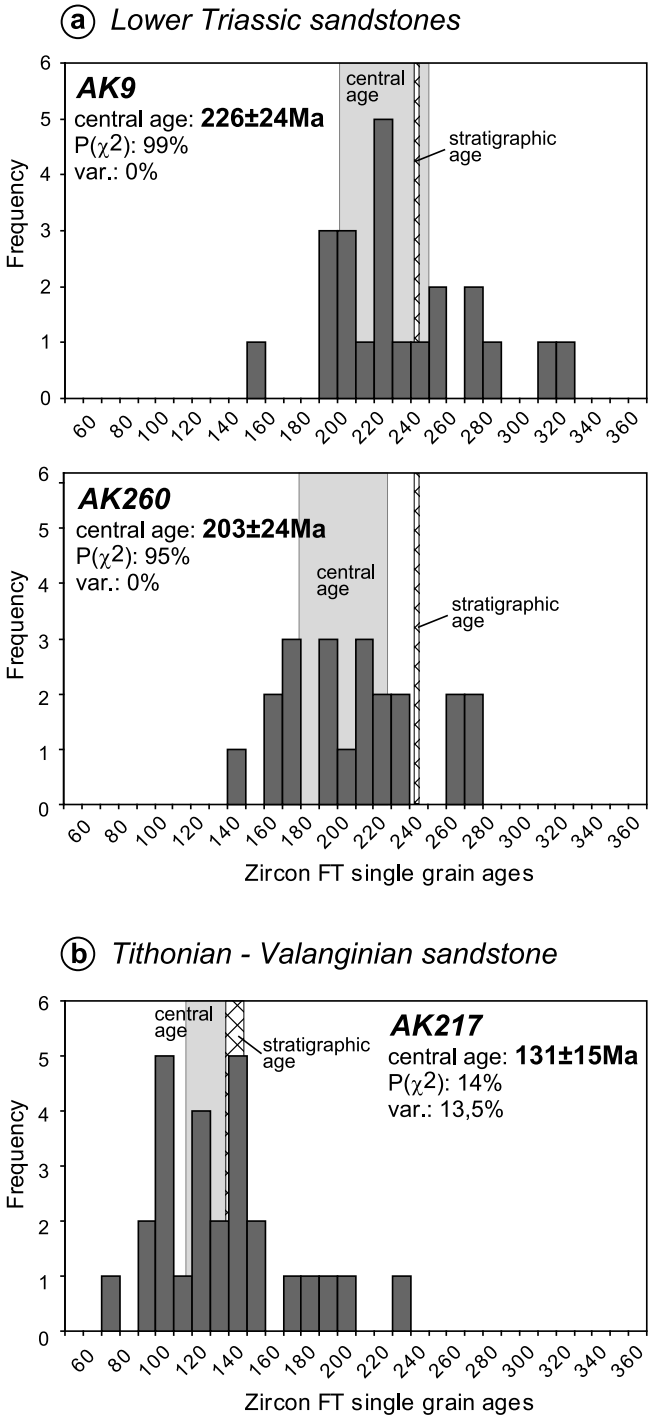

Figure 9. Frequency distribution of the zircon single-grain ages from (a) Lower Triassic sandstone samples AK09 and AK260 and (b) Tithonian–Valanginian turbidites (sample AK217).

units before and during the Cretaceous shortening and their subsequent cooling history.

5.1. Early Cretaceous Thrusting

[37] The internal zones of the Balkanides, including Rhodope, were dominated by compression until Cenomanian–Turonian time (circa 90 Ma) [*Ricou et al.*, 1998 *Sandulescu*, 1984; *Dimitrijević*, 1997]. In the Carpathians, compression ended between the Aptian and the earliest Cenomanian (125–100 Ma) [*Sandulescu*, 1984; *Dimitrijević*, 1997; *Schmid et al.*, 2008], and in the central Balkanides, the Late Jurassic–Early Cretaceous Troian basin evolved toward shallower facies and closure in pre-Albian time (i.e., before circa 110 Ma) [*Gocev*, 1982]; the only previously published geochronological datum from the Kraishte related to Cretaceous thrusting, is the 119 Ma K/Ar age of low-grade mylonites in the thrust zone [*Lilov and Zagorchev*, 1993]. We therefore may assume that compression in the Kraishte area was roughly contemporaneous with that in other areas of the internal Balkanides. Only the opening of the Sredna Gora back-arc basin in the Turonian–Campanian (circa 90–70 Ma) is evidence of a change to an extensional tectonic mode.

5.1.1. Morava Nappe

[38] All samples from the Morava nappe, with the exception of AK106, yield post-Valanginian (the lower stratigraphic bracket for nappe emplacement) zircon FT ages ranging between 119 and 78 Ma. They overlap with, or are younger than the upper time bracket proposed for the Cretaceous thrusting (Table 1 and Figures 3 and 10a). Sample AK106 (139 ± 15 Ma) has the oldest age. This sample comes from the upper part of the Morava nappe and may not have experienced temperatures high enough to reset the zircon FT age during the main shortening-thickening phase (group A, Figure 10b). The age may simply represent a cooling age of the rock before nappe stacking or, more probably, erosion-denudation of the Morava nappe during early thrusting. The fact that the sample comes from an undeformed granite boulder in a Paleogene breccia supports this idea because it is with all probability derived from the higher structural parts of the Morava unit already eroded during the Paleogene.

[39] It is difficult to say whether the ages of the other samples (Figure 10a) are related to cooling during erosion of the emplacing allochthon or posttectonic cooling associated with the overall denudation of the area. That some ages are similar to those from the autochthonous Struma Diorites favors the second suggestion. In either case, it is clear that before or during compression these rocks were at >~260°C, the temperature necessary for a full resetting (group B, Figure 10b). The oldest FT age from group B samples places the lower age bracket for thrusting at about 119 Ma (Aptian, Figure 10).

[40] The temperature estimates presented here are consistent with those suggested by *Graf* [2001] for the Cretaceous deformation phase in the Morava unit. He related the two movement phases he could distinguish to the low-grade overprint of the greenschist facies structures. To the southwest of Osogovo Mountain, Cretaceous deformation penetratively reworked older structures of the Morava unit. The

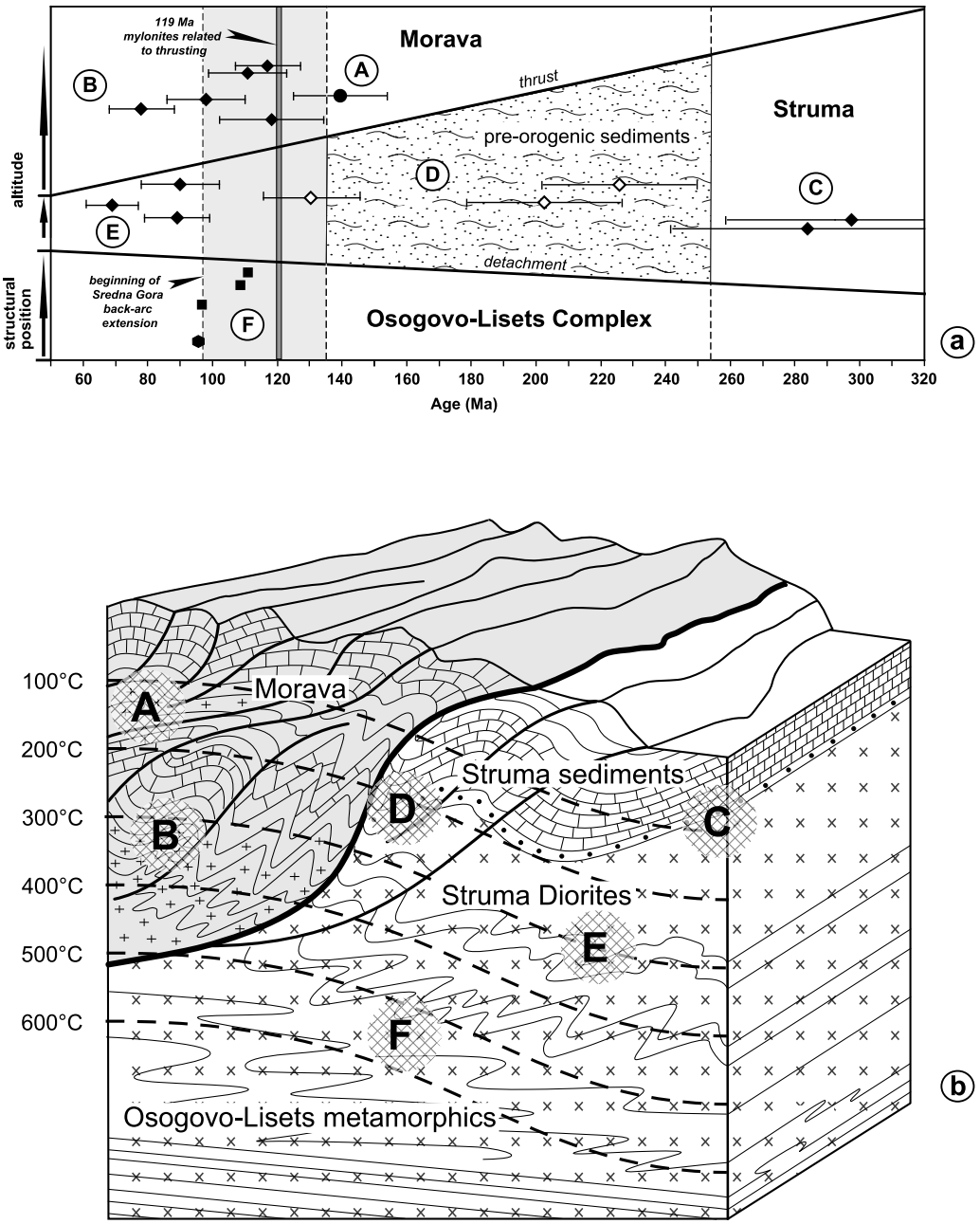

Figure 10. (a) Zircon FT and $^{40}Ar/^{39}Ar$ ages from the different units in the study area versus their structural position and altitude. Solid diamonds, zircon FT ages (groups B, C, and E); solid circle, zircon FT age (group A); empty diamonds, partially reset zircon FT ages (group D); solid squares, white mica $^{40}Ar/^{39}Ar$ ages (group F); solid hexagons, hornblende $^{40}Ar/^{39}Ar$ ages (group F). (b) Sketch of block diagram showing the relative position of the analyzed samples during thrusting.

foliation planes dip NW to SW with a NE trending lineation (Figure 4). Top-to-the-NE tectonic transport is similar to that in the Osogovo-Lisets metamorphic rocks (Figure 7). This may be because this area exposes deep structural levels of the Morava nappe with a higher degree of metamorphism and deformation than the Morava rocks in the northern part of the study area (Figure 11).

5.1.2. Struma Unit

[41] Two undeformed diorite samples from the eastern part of the study area yielded overlapping zircon FT ages of 298 ± 39 (AK229) and 284 ± 42 (AK113) (Figures 3 and 9a) suggesting that they have not experienced temperatures > 170–230°C since the Early Permian. This implies that the front of the Morava nappe was located to the west of this

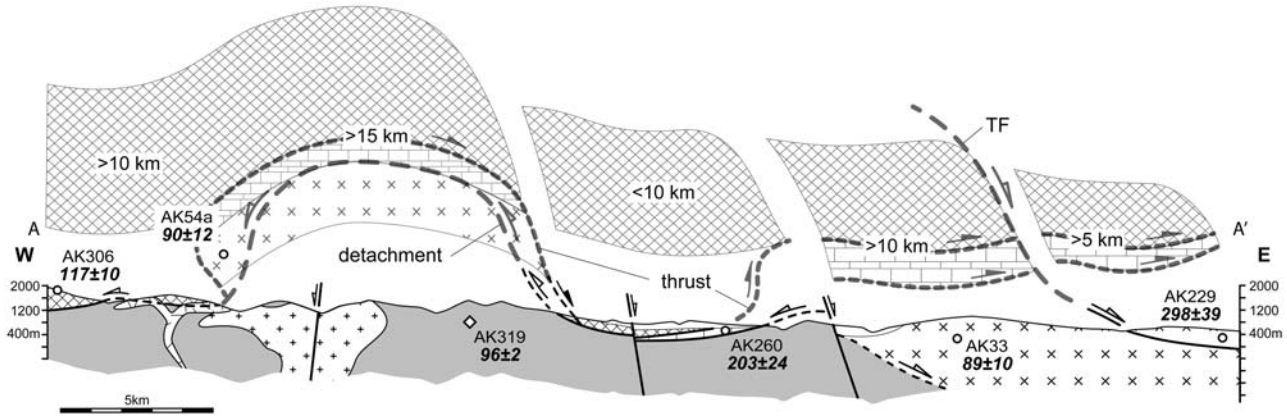

Figure 11. Section AA′ (Figure 3) across the Osogovo Mountain with zircon FT (circles) and $^{40}Ar/^{39}Ar$ (diamonds) ages. Estimated overburden of different parts of the section is also shown. Lithological key is as in Figure 3. TF, Tsurvishte fault. Location is AA′ line in Figure 3.

region or that its thickness was insufficient to bury rocks at resetting depth/temperatures of zircon (group C, Figure 10b).

[42] The samples from the Struma sedimentary cover have zircon FT ages between 226 and 131 Ma (Table 1 and Figure 10a), older than the time suggested for the thrusting event. The central ages are close to, and statistically overlap with the age of sedimentation (Figure 9), but single grain ages yield a relatively large spread with ages younger, equal and older than the depositional age (Figure 9). That some grains are younger than the stratigraphic age of the rock yields evidence that these rocks have undergone partial resetting during a thermal event younger than their apparent central ages (Figure 10a). Heating may result from tectonic burial below the Morava nappe overriding the Mesozoic sediments of the Struma unit; however, as argued before, the thickness of the nappe was insufficient to bury the sediments to the temperature needed (~260°C) to fully reset the zircon FT system (group D, Figure 10b).

[43] Three variously deformed Struma Diorite samples yield zircon FT ages between 90 and 69 Ma (group E, Figure 10a). These ages confirm that these samples were at deeper levels than the partially reset sediments and experienced temperatures >~260°C during thrusting-related burial (group E, Figure 10b).

5.1.3. Osogovo-Lisets Metamorphic Complex

[44] White mica growing on the foliation plane has $^{40}Ar/^{39}Ar$ plateau ages between 112 ± 1 and 97 ± 1 Ma and recrystallized hornblende has an age of 96 ± 2 Ma, suggesting that temperatures >~500°C were reached during deformation [*McDougall and Harrison*, 1999] (group F, Figure 10b). Structural and geochronological data suggest that the main metamorphic and deformational event associated with top-to-the-NE tectonic transport took place during the Early Cretaceous. The metamorphic peak was reached before 112 Ma, the oldest $^{40}Ar/^{39}Ar$ age obtained from the Osogovo-Lisets Metamorphic Complex.

[45] From the late Early Cretaceous until the onset of the Cenozoic extension, the presently exposed rocks probably resided at temperatures >~260°C because the zircon FT ages are all younger than ~50 Ma [*Kounov et al.*, 2004].

5.1.4. Ograzden Unit

[46] The tectonic position of the Ograzden unit during the Cretaceous orogeny remains unclear. If considered as part of the Serbo-Macedonian Massif in the sense of *Dimitrijević* [1967] and *Schmid et al.* [2008], the Ograzden unit belongs, together with the Morava unit to the allochthon of the thrust system. On the other hand, according to *Ricou et al.* [1998], the Ograzden is part of the Rhodope Complex and was exhumed from below the Struma unit along pre-~73 Ma flat-lying fault zones; in this interpretation, Ograzden was the lowermost tectonic unit of the Kraishte area. Our new thermochronological data shed some light on this controversy.

[47] The calculation of a reasonable plateau age from $^{40}Ar/^{39}Ar$ analyses for the white mica and biotite fractions from sample AK228 (Figure 8) was not possible. For white mica an age of ~160 Ma was obtained from the last six high-temperature gas-release steps (Figure 8). This age may be related to the cooling of the unit in the Middle to Late Jurassic. *Reischmann and Kostopoulos* [2001] reported an UHP metamorphic event at ~185 Ma followed by exhumation to lower crustal levels at about 145 ± 22 for the Serbo-Macedonian Massif of northern Greece. The biotite $^{40}Ar/^{39}Ar$ analysis suggests an initial isotopic closure at ~80 Ma, followed by partial resetting due to a later thermal event at ~30 Ma (Figure 8). Such a thermal history is in line with the zircon (88 ± 9 Ma, Figure 3) and apatite (31 ± 3 Ma [*Kounov*, 2002]) FT data obtained from the same sample. The 30 Ma thermal overprint is most likely related to magmatic activity at that time [*Kounov et al.*, 2004]. Both the $^{40}Ar/^{39}Ar$ and FT analyses suggest that the Ograzden unit reached temperatures higher than ~350°C in Cretaceous times.

[48] These geochronological data show that the Alpine geological evolution of the Ograzden is not that of the

Serbo-Macedonian Massif of Serbia. There, the Upper Complex of greenschist facies rocks [*Dimitrijević*, 1967] is unconformably overlain by undeformed Mesozoic sediments [*Andjelković*, 1976] and, therefore, did not experience any Alpine ductile deformation. The Ograzden Unit is better correlated with the Vertiskos and Kerdilion units of northern Greece, which are considered to be parts of the Serbo-Macedonian Massif that have experienced penetrative Alpine deformation, like the Rhodope [*Burg et al.*, 1995]. Indeed the "pre-~73 Ma" Gabrov Dol detachment [*Bonev et al.*, 1995] separating the Ograzden gneisses from the Struma basement in our study area must be older than ~90 Ma, as constrained by identical zircon FT ages determined on both sides of the fault (Figure 3).

5.2. Late Cretaceous Denudation

[49] The zircon FT and $^{40}Ar/^{39}Ar$ data are cooling ages postdating the peak of metamorphic temperatures at >500°C (amphibolite facies). This leads to the conclusion that nappe stacking in the Osogovo-Lisets Complex took place before 112 Ma (the oldest $^{40}Ar/^{39}Ar$ age from the overthrust footwall). It is however difficult to date the exact onset of cooling or to calculate cooling rates. This is because faulting during at least two stages of Cenozoic extension has cut out significant portions of the section, thus hampering the reconstruction of Cretaceous isotherms [*Kounov et al.*, 2004].

[50] The exhumation mechanism and the tectonic setting of the Kraishte area after thrusting are difficult to reconstruct. The Kraishte is situated on the southwestern border of the Late Cretaceous Sredna Gora back-arc basin and, therefore, the back-arc extension that affected that region may have expanded to, and included the Kraishte area. The previously reported Gurbino-Zlogosh and Tsurvishte low-angle normal faults (Figure 3) [*Bonev et al.*, 1995; *Graf*, 2001] probably were active all that time as indicated by considerably younger zircon FT ages in footwall samples (Figure 3, 89 ± 10 Ma (AK33), 69 ± 8 Ma (K93) and 88 ± 9 Ma (AK228)) than in the hanging wall (Figure 3, 131 ± 15 Ma (AK217), 284 ± 42 Ma (AK113) and 298 ± 39 Ma (AK229)).

6. Conclusions

[51] Top-to-the-NE directed nappe stacking in the Kraishte area of the Balkan orocline was associated with lower amphibolite facies metamorphism and deformation between 139 and 112 Ma in the Osogovo-Lisets Metamorphic Complex (Figure 11).

[52] The Valanginian (140–136 Ma) cessation of sedimentation in Struma unit marks the onset of thrusting of the Morava onto the Struma. During this 139–112 Ma tectonic and metamorphic event, the Morava nappe experienced temperature >~260°C, which left a widespread, low-grade overprint. The structurally intermediate Struma Diorites and their Mesozoic cover experienced temperatures between ~170°C and 300°C (Figure 11). Recorded temperatures decreased northeastward and up section, probably reflecting decreasing depths during the Cretaceous. The present-day juxtaposition of the Morava and Struma units with the Osogovo-Lisets metamorphic dome is related to low-angle normal faulting during Cenozoic extension (45–30 Ma).

Appendix A

A1. Fission Track

[53] Sample preparation followed the routine technique described by *Seward* [1989]. Zircon grains were etched in a eutectic mixture of KOH and NaOH at 220°C for between 4 and 40 h. Irradiation was carried out at the ANSTO facility, Lucas Heights, Australia.

[54] Microscopic analysis was completed at ETH, Zurich using an optical microscope with a Kinetek computer-driven stage [*Dumitru*, 1993]. All ages were determined (analyst: A. Kounov) using the zeta approach [*Hurford and Green*, 1983] with a zeta value of 132 ± 3 (CN1 standard glass; Table 1). They are reported as central ages [*Galbraith and Laslett*, 1993] with a 2σ error (Table 1). The magnification used was x1600 (dry).

A2. The $^{40}Ar/^{39}Ar$ Ratio

[55] For $^{40}Ar/^{39}Ar$ dating mineral concentrates were packed in aluminum foil and loaded in quartz vials (see Table A1). For calculation of the J values, flux monitors were placed between each four to five unknown samples, which yielded a distance of *c*. Five mm between adjacent flux monitors. The sealed quartz vials were irradiated in the MTA KFKI reactor (Debrecen, Hungary) for 16 h. Correction factors for interfering isotopes have been calculated from 10 analyses of two Ca-glass samples and 22 analyses of two pure K-glass samples, and are: $^{36}Ar/^{37}Ar_{(Ca)} = 2.6025 \times 10^{-4}$, $^{39}Ar/^{37}Ar_{(Ca)} = 6.5014 \times 10^{-4}$, and $^{40}Ar/^{39}Ar_{(K)} = 1.5466 \times 10^{-2}$. Variations in the flux of neutrons were monitored with the DRA1 sanidine standard for which a $^{40}Ar/^{39}Ar$ plateau age of 25.03 ± 0.05 Ma has been reported [*Wijbrans et al.*, 1995]. After irradiation the minerals are unpacked from the quartz vials and the aluminum foil packets, and handpicked into 1 mm diameter holes within one-way Al sample holders.

[56] The $^{40}Ar/^{39}Ar$ analyses were carried out at the Department for Geography and Geology at the University Salzburg by R Handler. UHV Ar extraction line equipped with a combined MERCHANTEK^{TM} UV/IR laser ablation facility and a VG-ISOTECH^{TM} NG3600 Mass Spectrometer were used.

[57] Stepwise heating analyses of samples were performed using a defocused (~1.5 mm diameter) 25 W CO_2-IR laser operating in Tem_{00} mode at wavelengths between 10.57 and 10.63 μm. The laser is controlled from a PC, and the position of the laser on the sample is monitored through a double-vacuum window on the sample chamber via a video camera in the optical axis of the laser beam on the computer screen. Gas clean-up is performed using one hot and one cold Zr-Al SAES getter. Gas admittance and pumping of the mass spectrometer and the Ar extraction line are computer controlled using pneumatic valves. The NG3600 is an 18 cm radius 60° extended geometry instrument, equipped with a bright NIER-type source operated at 4,5 kV. Measurement is performed on an axial electron multiplier in static mode,

Table A1. Summary of the $^{40}Ar/^{39}Ar$ Isotopic Data From All Dated Samples

	$^{36}Ar/^{39}Ar$		$^{37}Ar/^{39}Ar$		$^{40}Ar/^{39}Ar$					
Step	Measured	1σ Absolute	Corrected	1σ Absolute	Measured	1σ Absolute	$^{40}Ar^{*}$ (%)	^{39}Ar (%)	Age (Ma)	$\pm$1σ Absolute (Ma)
AK3, White Mica, J Value 0.0197 ± 0.0002										
1	0.003081	0.000136	0.149897	0.000138	3.49567	0.04016	74	3.3	89.5	1.6
2	0.001985	0.000085	0.211083	0.00009	3.52684	0.02503	83.4	5.8	101.6	1.3
3	0.000932	0.000034	0.195394	0.000054	3.33384	0.01004	91.7	12	105.6	1.1
4	0.000593	0.000034	0.464231	0.000064	3.23911	0.0101	94.6	13.5	106.4	1.1
5	0.000289	0.000016	0.111008	0.000021	3.21907	0.00462	97.3	30.1	107.8	1.1
6	0.000628	0.000094	0.008952	0.000084	3.35269	0.02777	94.5	4.1	108.7	1.4
7	0.000304	0.000024	0.003736	0.000024	3.25521	0.00713	97.2	14.8	108.6	1.1
8	0.000144	0.000037	0.002501	0.000039	3.21538	0.01106	98.7	10.8	108.9	1.1
9	0.000063	0.00011	0.003578	0.00014	3.26714	0.03252	99.4	2.9	111.4	1.5
10	0.000108	0.000098	0.004039	0.000157	3.39593	0.02909	99.1	2.7	115.3	1.5
4–8								73.2	108.03	0.51
9	0.0009	0.00004	0.001265	0.000033	3.10694	0.0119	91.4	12.6	97.1	1
10	0.00125	0.000081	0.006265	0.000053	3.1905	0.02392	88.4	5.9	96.4	1.2
11	0.000973	0.000037	0.00182	0.000029	3.10508	0.01108	90.7	14.2	96.3	1
12	0.000465	0.000245	0.004386	0.000267	3.01183	0.07258	95.4	1.7	98.2	2.6
5–12								80.4	97.31	0.41
AK228, White Mica, J Value 0.01966 ± 0.0002										
1	0.008851	0.000236	0.016221	0.000181	5.7221	0.06978	54.3	0.8	106.5	2.6
2	0.002033	0.000137	0.008832	0.000123	4.70082	0.04061	87.2	1.3	139.4	1.9
3	0.001712	0.000322	0.018417	0.000282	4.26055	0.0954	88.1	0.5	128	3.4
4	0.000701	0.000048	0.004378	0.000051	5.59616	0.01442	96.3	3	181.2	1.8
5	0.000267	0.000202	0.011106	0.000257	3.98603	0.05995	98	0.6	133	2.4
6	0.000405	0.000022	0.00164	0.000019	9.10173	0.00671	98.7	7.8	292.9	2.7
7	0.000184	0.000028	0.002733	0.000027	5.01858	0.00822	98.9	5.3	167.5	1.6
8	0.00033	0.000012	0.001407	0.00001	6.23508	0.00369	98.4	14.4	205	1.9
9	0.000132	0.00001	0.000263	0.000007	5.13923	0.00295	99.2	18.6	171.9	1.6
10	0.000094	0.000009	0.000393	0.000007	4.6931	0.00275	99.4	19.8	157.8	1.5
11	0.000158	0.000026	0.000717	0.000019	4.77312	0.00771	99	6.5	159.8	1.5
12	0.000141	0.000019	0.002691	0.000013	4.81706	0.00553	99.1	8.9	161.4	1.6
13	0.000075	0.000041	0.003488	0.000033	4.87825	0.01227	99.5	3.7	164	1.6
14	0.000052	0.000033	0.000725	0.000029	4.82458	0.00971	99.7	4.8	162.5	1.6
15	0.000015	0.000039	0.004245	0.000038	4.61168	0.01161	99.9	3.9	155.9	1.5
AK347, White Mica, J Value 0.0197 ± 0.0002										
1	0.009833	0.000385	0.018972	0.000319	5.13848	0.11397	43.5	1	77.2	4
2	0.001498	0.000047	0.003627	0.000045	3.71592	0.01403	88.1	7.4	112.2	1.2
3	0.0005	0.000033	0.002326	0.000032	3.4793	0.00977	95.8	9.7	114.2	1.2
4	0.000698	0.000132	0.001711	0.000164	3.44199	0.03899	94	1.8	111	1.7
5	0.000663	0.00005	0.005287	0.000055	3.44765	0.0149	94.3	6	111.5	1.2
6	0.000662	0.000042	0.003414	0.000048	3.4894	0.01241	94.4	6.3	112.9	1.2
7	0.000294	0.000025	0.002473	0.000024	3.40284	0.00747	97.5	13.2	113.7	1.1
8	0.000273	0.000038	0.00392	0.000047	3.36104	0.0113	97.6	6.3	112.5	1.2
9	0.000204	0.000018	0.001795	0.000022	3.31691	0.0053	98.2	15.8	111.7	1.1
10	0.000084	0.000133	0.007214	0.000122	3.25344	0.03938	99.2	2.2	110.7	1.7
11	0.000193	0.000058	0.00432	0.000057	3.32553	0.01711	98.3	5.4	112.1	1.2
12	0.000179	0.000036	0.003417	0.000033	3.26709	0.01068	98.4	8.8	110.3	1.1
13	0.000124	0.000026	0.001377	0.000028	3.48113	0.00779	98.9	10.2	117.9	1.2
14	0.000027	0.000047	0.013269	0.000051	3.47288	0.01398	99.8	5.9	118.6	1.2
2–12								82.9	112.19	0.37
AK228, Biotite, J Value 0.0197 ± 0.0002										
1	0.108018	0.000279	0.023266	0.000095	32.8031	0.08427	2.7	1.6	30.7	3
2	0.035604	0.000078	0.012203	0.000024	12.1442	0.0231	13.4	7.7	56.3	1
3	0.016484	0.000107	0.012663	0.000056	6.66352	0.03182	26.9	2.9	62.1	1.3
4	0.017074	0.000055	0.010573	0.000019	7.04984	0.01625	28.4	9.7	69.4	0.9
5	0.012487	0.000061	0.011232	0.000037	5.76295	0.01809	36	4.3	71.7	0.9
6	0.012379	0.00003	0.010132	0.000022	5.96083	0.00886	38.6	8.3	79.5	0.8
7	0.011642	0.000039	0.010427	0.000014	5.80409	0.01162	40.7	13.1	81.6	0.9
8	0.011808	0.000058	0.011969	0.000033	5.76331	0.01724	39.5	4.9	78.6	1
9	0.012666	0.000077	0.012389	0.000028	6.07409	0.02276	38.4	5.4	80.5	1.1
10	0.013525	0.000106	0.014486	0.000075	6.22299	0.03132	35.8	2.1	77	1.3
11	0.009691	0.000064	0.013423	0.000026	5.08587	0.01901	43.7	5.3	76.8	1
12	0.009494	0.000105	0.013027	0.000075	5.03233	0.03107	44.2	2.1	77	1.3
13	0.009261	0.000082	0.009893	0.000051	4.99001	0.02427	45.2	3.3	77.9	1.1
14	0.00858	0.000054	0.009112	0.000027	4.90647	0.01588	48.3	5.5	81.9	1
15	0.008667	0.000038	0.010555	0.000017	4.92904	0.01121	48	9.8	81.8	0.9
16	0.008653	0.000062	0.011057	0.000035	4.82155	0.01843	47	4.6	78.2	1
17	0.007985	0.000055	0.020539	0.000022	4.74572	0.01622	50.3	5.8	82.4	1
18	0.007751	0.000086	0.0763	0.00005	4.60307	0.02541	50.2	3.4	80.1	1.2

Table A1. (continued)

Step	$^{36}Ar/^{39}Ar$ Measured	$^{36}Ar/^{39}Ar$ 1σ Absolute	$^{37}Ar/^{39}Ar$ Corrected	$^{37}Ar/^{39}Ar$ 1σ Absolute	$^{40}Ar/^{39}Ar$ Measured	$^{40}Ar/^{39}Ar$ 1σ Absolute	$^{40}Ar^{*}$ (%)	^{39}Ar (%)	Age (Ma)	±1σ Absolute (Ma)
AK319, Hornblende, J Value 0.0197 ± 0.0002										
1	0.048586	0.005296	0.508286	0.004158	18.3121	1.57413	21.6	0.6	136.2	51.9
2	0.026773	0.002163	11.318634	0.01217	9.44712	0.64118	16.3	1.1	83.6	21.8
3	0.01134	0.000275	13.724904	0.002523	4.42241	0.08144	24.2	11.4	74.2	2.9
4	0.007848	0.000226	15.092682	0.002188	3.92422	0.06681	40.9	14.1	96.1	2.4
5	0.005067	0.000083	15.3728	0.000955	3.07558	0.02456	51.3	47.4	96	1.2
6	0.007124	0.000997	13.41909	0.006977	4.2507	0.29491	50.5	2.9	110	9.9
7	0.006291	0.000192	15.522356	0.002273	3.30895	0.05689	43.8	15.3	92	2.1
8	0.003504	0.000337	15.574799	0.003973	2.75452	0.09968	62.4	6.9	101.3	3.5
9	0.008183	0.00523	16.013149	0.031153	3.19578	1.5461	24.3	0.5	70.2	52.9
4–9								87	95.7	0.94

peak jumping and stability of the magnet is controlled by a Hall probe. For each increment the intensities of ^{36}Ar, ^{37}Ar, ^{38}Ar, ^{39}Ar and ^{40}Ar are measured, the baseline readings on mass 35.5 are automatically subtracted. Intensities of the peaks are back-extrapolated over 16 measured intensities to the time of gas admittance either by a straight line or a curved fit. Intensities are corrected for system blanks, background, postirradiation decay of ^{37}Ar, and interfering isotopes. Isotopic ratios, ages and errors for individual steps are calculated following suggestions by *McDougall and Harrison* [1999] using decay factors reported by *Steiger and Jäger* [1977]. Definition and calculation of plateau ages have been carried out using ISOPLOT/EX [*Ludwig*, 2001].

[58] **Acknowledgments.** This study was supported by the ETH Zurich, project 0-20657-99. The University of Sofia supported Z. Ivanov. We thank the entire Structural Geology and Tectonic research group from Sofia University, Bulgaria, for their advice and particularly their support in the field. Constructive reviews by Clark Burchfiel and Giulio Viola have helped to improve the quality of the paper.

References

Andjelković, M. (1976), Moravska zona, in *Géologie de la Serbie*, edited by K. Petkovic, pp. 184–185, Univ. de Belgrade, Belgrade.

Aubouin, J., M. Bonneau, J. Davidson, P. Leboulanger, S. Matesco, and A. Zambetakis (1976), Esquisse structurale de l'arc égéen externe: Des Dinarides aux Taurides, *Bull. Geol. Soc. Fr.*, *7*(17), 131–140.

Baumgartner, P. O. (1985), *Jurassic sedimentary evolution and nappe emplacement in the Argolis Peninsula (Peloponnesus; Greece)*, *Mem. Soc. Helv. Sci. Nat.*, 99, 111 pp.

Belmoustakov, E. (1948), La géologie de la partie méridionale de la région Pianec (Bulgarie), *Rev. Bulgarian Geol. Soc.*, *20*, 1–63.

Bernoulli, D. (2001), Mesozoic-Tertiary carbonate platforms, slopes and basins of the external Apennines and Sicily, in *Anatomy of a Orogen: The Apennines and Adjacent Mediterranean Basins*, edited by G. B. Vai and P. Martini, pp. 307–325, Kluwer Acad., Dordrecht, Netherlands.

Bernoulli, D., and H. Laubscher (1972), The palinspastic problem of the Hellenides, *Eclogae Geol. Helv.*, *65*, 107–118.

Boccaletti, M., P. Manetti, and A. Peccerillo (1974), The Balkanides as an instance of back-arc thrust belt: Possible relation with the Hellenides, *Geol. Soc. Am. Bull.*, *85*, 1077–1084, doi:10.1130/0016-7606(1974)85<1077:TBAAIO>2.0.CO;2.

Bonchev, E. (1936), Versuch einer tektonischen Synthese Westbulgariens, *Geol. Balcanica*, *2*, 5–48.

Bonchev, E. (1986), *Balkanides—Geotectonic Position and Development*, 273 pp., Bulg. Acad. Sci., Sofia.

Bonev, K., Z. Ivanov, and L.-E. Ricou (1995), Dénudation tectonique au toit du noyau métamorphique rhodopien-macédonien: La faille normale ductile de Gabrov Dol (Bulgarie), *Bull. Soc. Geol. Fr.*, *166*, 49–58.

Bott, M. H. P. (1959), The mechanics of oblique slip faulting, *Geol. Mag.*, *96*, 109–117, doi:10.1017/S0016756800059987.

Burchfiel, C. B., R. Nakov, N. Domurdzanov, D. Papanikolau, T. Tzankov, T. Serafimovski, R. W. King, V. Kotzev, A. Todosov, and B. Nurce (2008), Evolution and dynamics of the Cenozoic tectonics of south Balkan extensional system, *Geosphere*, *4*(6), doi:10.1130/GES00169.1.

Burg, J.-P., I. Godfriaux, and L.-E. Ricou (1995), Extension of the Mesozoic Rhodope thrust units in the Vertiskos-Kerdilion Massifs (northern Greece), *C. R. Acad. Sci., Ser. 2*, *320*, 889–896.

Burg, J.-P., L.-E. Ricou, Z. Ivanov, I. Godfriaux, D. Dimov, and L. Klain (1996), Synmetamorphic nappe complex in the Rhodope Massif: Structure and kinematics, *Terra Nova*, *8*, 6–15, doi:10.1111/j.1365-3121.1996.tb00720.x.

Channell, J. E. T., and F. Horvath (1976), The African/Adriatic Promontory as a paleogeographical premise for Alpine orogeny and plate movements in the Carpatho-Balkan region, *Tectonophysics*, *35*, 71–101, doi:10.1016/0040-1951(76)90030-5.

Compton, R. R. (1966), Analyses of Pliocene-Pleistocene deformation and stresses in northern Santa Lucia Range, California, *Geol. Soc. Am. Bull.*, *77*, 1361–1379, doi:10.1130/0016-7606(1966)77[1361:AOPDAS]2.0.CO;2.

Coyle, D. A., and G. A. Wagner (1998), Positioning the titanite fission-track partial annealing zone, *Chem. Geol.*, *149*, 117–125, doi:10.1016/S0009-2541(98)00041-2.

Dabovski, C., I. Boyanov, K. Khrischev, T. Nikolov, I. Sapounov, Y. Yanev, and I. Zagorchev (2002), Structure and Alpine evolution of Bulgaria, *Geol. Balcanica*, *32*, 2–4, 9–15.

Dallmeyer, R. D., F. Neubauer, R. Handler, H. Fritz, W. Müller, D. Pana, and M. Putiš (1996), Tectonothermal evolution within the internal Alps and Carpathians: Evidence from $^{40}Ar-^{39}Ar$ mineral and whole-rock data, *Eclogae Geol. Helv.*, *89*, 203–227.

Dercourt, J., and L.-E. Ricou (1987), Discussion sur la place de la Bulgarie au sein du systeme alpin, *Rev. Bulgarian Geol. Soc.*, *48*, 1–14.

Dercourt, J., et al. (1986), Geological evolution of the Tethys belt from the Atlantic to the Pamir since the Lias, *Tectonophysics*, *123*, 241–315, doi:10.1016/0040-1951(86)90199-X.

Dewey, J. F., W. C. Pitman III, W. B. F. Ryan, and J. Bonin (1973), Plate tectonics and the evolution of the Alpine system, *Geol. Soc. Am. Bull.*, *84*, 3137–3180, doi:10.1130/0016-7606(1973)84<3137:PTATEO>2.0.CO;2.

Dimitrijević, M. D. (1967), Some problems of crystalline schists in the Serbo-Macedonian Massif, in *VIII Congress Reports Petrology and Metamorphism*, pp. 59–67, Carpatho-Balkan Geol. Assoc., Bucharest.

Dimitrijević, M. D. (1997), *Geology of Yugoslavia*, Geol. Inst. GEMINI, Belgrade.

Dimitrov, C. (1931), Contribution to the geology and petrography of the Konyavo Mountain (in Bulgarian), *Rev. Bulgarian Geol. Soc.*, *3*, 3–52.

Dimitrova, E. (1964), Petrologie des kristallinen Sockels des Osogovo Gebirges, *Bull. Geol. Inst. Ser. Stratigr. Lithol.*, *13*, 99–110.

Dinter, D. A., and L. Royden (1993), Late Cenozoic extension in northeastern Greece: Strymon Valley detachment system and Rhodope metamorphic core complex, *Geology*, *21*, 45–48, doi:10.1130/0091-7613(1993)021<0045:LCEING>2.3.CO;2.

Dumitru, T. A. (1993), A new computer automated microscope stage system for fission-track analysis, *Nucl. Tracks Radiat. Meas.*, *21*, 575–580, doi:10.1016/1359-0189(93)90198-I.

Etchecopar, A., G. Vassuer, and M. Daignieres (1981), An inverse problem in microtectonics for the determination of stress tensor from fault striations analysis, *J. Struct. Geol.*, *3*, 51–65, doi:10.1016/0191-8141(81)90056-0.

Galbraith, R. F. (1981), On statistical-models for fission track counts, *J. Int. Assoc. Math. Geol.*, *13*, 471–478, doi:10.1007/BF01034498.

Galbraith, R. F., and G. M. Laslett (1993), Statistical models for mixed fission-track ages, *Nucl. Tracks Radiat. Meas.*, *21*, 459–470, doi:10.1016/1359-0189(93)90185-C.

Gocev, P. M. (1982), On the problem of Alpine zoning, vergence and other features of nappes in Bulgaria and eastern part of the Balkan peninsula, in *Alpine Structural Elements: Carpathian-Balkan-Caucasus-Pamir Orogen Zone*, edited by M. Mahel, pp. 75–93, Slovak Acad. of Sci., Veda.

Graf, J. (2001), Alpine tectonics in western Bulgaria: Cretaceous compression of the Kraishte region

and Cenozoic exhumation of the crystalline Osogovo-Lisets Complex, Ph.D. thesis, 183 pp., ETH Zurich, Zürich.

Green, P. F., K. A. Hegarty, I. R. Duddy, S. S. Foland, and V. Gorbachev (1996), Geological constraints on fission track annealing in zircon, paper presented at International Workshop on Fission Track Dating, Geol. Inst. and Inst. for Nucl. Sci., Univ. of Ghent, Ghent, Belgium.

Harkovska, A., and Z. Pecskay (1997), The Tertiary magmatism in Ruen magmato-tectonic zone (W. Bulgaria)—A comparison of new K-Ar ages and geological data, in *Magmatism, Metamorphism and Metallogeny of the Vardar Zone and Serbo-Macedonian Massif*, edited by B. Boev and T. Serafimovski, pp. 137–142, Fac. of Min. Geol., Stip-Dojran, Macedonia.

Hasebe, N., S. Mori, T. Tagami, and R. Matsui (2003), Geological partial annealing zone of zircon fission-track system: Additional constraints from the deep drilling MITI-Nishikubiki and MITI-Mishima, *Chem. Geol.*, *199*, 45–52.

Haydoutov, I., K. Kolcheva, and L. Daieva (1994), The Struma Diorite Fm from Vlahina block, SW Bulgaria, *Rev. Bulgarian Geol. Soc.*, *55*, 9–35.

Hurford, A. J., and P. F. Green (1983), The zeta age calibration of fission-track dating, *Isot. Geosci.*, *1*, 285–317.

Kober, L. (1952), *Leitlinen der Tektonik Jugoslawiens, Posebna Izdanja SAN 189*, pp. 1–64, Geol. Inst., Belgrade.

Kounov, A. (2002), Thermotectonic evolution of Kraishte, western Bulgaria, Ph.D. thesis, 219 pp., ETH Zurich, Zürich.

Kounov, A., D. Seward, D. Bernoulli, J.-P. Burg, and Z. Ivanov (2004), Thermotectonic evolution of an extensional dome: The Cenozoic Osogovo-Lisets core complex (Kraishte zone, western Bulgaria), *Int. J. Earth Sci.*, *93*, 1008–1024, doi:10.1007/s00531-004-0435-2.

Kräutner, H. G., and B. Kristić (2002), Alpine and pre-Alpine structural units within the southern Carpathians and western Balkanides, *Geol. Carpathica*, *53*, Spec. Issue.

Kristić, B., S. Karamata, and V. Milićević (1996), The Carpatho-Balkanide terranes—A correlation, in *Terranes of Serbia: The Formation of the Geologic Framework of Serbia and The Adjacent Regions*, edited by V. Knezević and B. Kristić, pp. 71–76, Fac. of Min. and Geol., Univ. of Belgrade, Belgrade.

Liati, A., D. Gebauer, and R. Wysoczanski (2002), U–Pb SHRIMP-dating of zircon domains from UHP garnet-rich mafic rocks and late pegmatoids in the Rhodope zone (N Greece): Evidence for Early Cretaceous crystallization and Late Cretaceous metamorphism, *Chem. Geol.*, *184*, 281–299, doi:10.1016/S0009-2541(01)00367-9.

Lilov, P., and I. Zagorchev (1993), K-Ar data for the deformation and low-grade metamorphism in Permian and Triassic red beds in SW Bulgaria, *Geol. Balcanica*, *23*, 46.

Ludwig, K. R. (2001), Isoplot/Ex—A geochronological toolkit for Microsoft Excel, *Spec. Publ. 1a*, 55 pp., Berkeley Geochronol. Cent., Berkeley, Calif.

McDougall, I. and T. M. Harrison (1999), *Geochronology and Thermochronology by the $^{40}Ar/^{39}Ar$ Method*, 2nd ed., 269 pp., Oxford Univ. Press, New York.

Moskovski, S. (1968), Tectonic of the Pianec grabens complex south of Kjustendil (in Russian), *Bull. Geol. Inst. Ser. Stratigr. Lithol.*, *17*, 143–158.

Moskovski, S., and V. Shopov (1965), Stratigraphy of the Paleogene and the resedimentation phenomena (olistostromes) related to it in Pyanets area, Kjustendil district (SW Bulgaria) (in Bulgarian, abstract in English), *Bull. Geol. Inst. Sofia Stratigr. Lithol.*, *16*, 189–209.

Nachev, I., and T. Nikolov (1968), The lower Cretaceous in the Kraishte (in Bulgarian), *Bull. Bulgarian Geol. Soc.*, *29*, 330–333.

Petrović, B. (1969), Structure of the Vlasina crystalline complex in the wider area of Crna Trava, Ph.D. thesis, Fac. of Min. and Geol., Univ. of Belgrade, Belgrade.

Reischmann, T., and D. Kostopoulos (2001), Geochronology and P-T constraints on the exhumation history of an UHP eclogite from northern Greece, *Eos Trans. AGU*, *82*(47), Fall. Meet. Suppl., Abstract V32C-0987.

Ricou, L.-E., J.-P. Burg, I. Godfriaux, and Z. Ivanov (1998), Rhodope and Vardar: The metamorphic and the olistostromic paired belts related to the Cretaceous subduction under Europe, *Geodin. Acta*, *11*, 285–309, doi:10.1016/S0985-3111(99)80018-7.

Sandulescu, M. (1984), *Geotectonics of Romania*, Tehnica, Bucharest.

Schmid, S. M., D. Bernoulli, B. Fügenschuh, L. Matenco, S. Schefer, R. Schuster, M. Tischler, and K. Ustaszewski (2008), The Alpine-Carpathian-Dinaridic orogenic system: Compilation and evolution of tectonic units, *Swiss J. Geosci.*, *101*, 139–183, doi:10.1007/s00015-008-1247-3.

Seward, D. (1989), Cenozoic basin histories determined by fission-track dating of basement granites, South Island, New Zealand, *Chem. Geol.*, *79*, 31–48.

Spassov, C. (1973), Stratigraphie des Devons in Sudwest-Bulgarien, *Bull. Geol. Inst. Ser. Stratigr. Lithol.*, *22*, 5–38.

Steiger, R. H., and E. Jäger (1977), Subcommission on Geochronology: Convention on the use of decay constants in geo- and cosmochronology, *Earth Planet. Sci. Lett.*, *36*, 359–362, doi:10.1016/0012-821X(77)90060-7.

Stephanov, A., and Z. Dimitrov (1936), Geologische Untersuchungen im Kustendiler Gebiet, *Rev. Bulgarian Geol. Soc.*, *8*, 1–28.

Tagami, T. (2005), Zircon fission-track thermochronology and applications to fault studies, in *Low-Temperature Thermochronology: Techniques, Interpretations, and Applications*, edited by P. W. Reiners and T. A. Ehlers, *Rev. Mineral. Geochem.*, *58*(1), 95–122, doi:10.2138/rmg.2005.58.4.

Tagami, T., and T. Dumitru (1996), Provenance and thermal history of the Franciscan accretionary complex: Constraints from zircon fission track thermochronology, *J. Geophys. Res.*, *101*, 11,353–11,364, doi:10.1029/96JB00407.

Tagami, T., A. Carter, and A. J. Hurford (1996), Natural long-term annealing of the zircon fission-track system in Vienna Basin deep borehole samples: Constraints upon the partial annealing zone and closure temperature, *Chem. Geol.*, *130*, 147–157, doi:10.1016/0009-2541(96)00016-2.

Tagami, T., R. F. Galbraith, R. Yamada, and G. M. Laslett (1998), Revised annealing kinetics of fission tracks in zircon and geological implications, in *Advances in Fission-Track Geochronology*, *Solid Earth Sci. Libr.*, vol. 10, edited by P. Van den Haute and F. de Corte, pp. 99–112Kluwer Acad., Norwell, Mass.

Velichkova, S. H., R. Handler, F. Neubauer, and Z. Ivanov (2004), Variscan to Alpine tectonothermal evolution of the Central Srednogorie Zone, Bulgaria: Constraints from $^{40}Ar/^{39}Ar$ analysis, *Schweiz. Mineral. Petrogr. Mitt.*, *84*, 133–151.

Wawrzenitz, N., and E. Mposkos (1997), First evidence for lower Cretaceous HP = HT-metamorphism in the eastern Rhodope, north Aegean region, north-east Greece, *Eur. J. Mineral.*, *9*, 659–664.

Wijbrans, J. R., M. S. Pringle, A. A. P. Koopers, and R. Schveers (1995), Argon geochronology of small samples using the Vulkaan argon laserprobe, *Proc. K. Ned. Akad. Wet.*, *98*, 185–218.

Yamada, R., T. Tagami, S. Nishimura, and H. Ito (1995), Annealing kinetics of fission tracks in zircon: An experimental study, *Chem. Geol.*, *122*, 249–258, doi:10.1016/0009-2541(95)00006-8.

Zagorchev, I. (1980), Early Alpine deformations in the red beds within the Poletinci-Skrino fault zone. I. Lithostratigraphic features in light of structural studies (in Russian, abstract in English), *Geol. Balcanica*, *10*, 37–60.

Zagorchev, I. (1984a), The importance of overthrusts in the Alpine structure of Kraistids (in Russian, abstract in English), *Geol. Balcanica*, *14*, 37–64.

Zagorchev, I. (1984b), Pre-Alpine structure of south–west Bulgaria (in Bulgarian), in *Problems of the Geology of Southwestern Bulgaria*, edited by I. Zagorchev, S. Mankov, and I. Bozkov, pp. 9–20, Tehnika, Sofia.

Zagorchev, I. (1993), Radomir and Bosilegrad map sheets: Explanatory notes, Geological map of Bulgaria on scale 1:100000, Bulg. Comm. of Geol., Sofia.

Zagorchev, I. (1995), Pre-Paleogene Alpine tectonics in southwestern Bulgaria, *Geol. Balcanica*, *25*, 91–112.

Zagorchev, I. (1996), Geological heritage of the Balkan Peninsula: Geological setting (an overview), *Geol. Balcanica*, *26*, 3–10.

Zagorchev, I. (2001), Introduction to the geology of SW Bulgaria, *Geol. Balcanica*, *31*, 3–52.

Zagorchev, I., and M. Ruseva (1982), Nappe structure of the southern parts of Osogovo Mts. and Pijanec region (SW Bulgaria) (in Russian, abstract in English), *Geol. Balcanica*, *12*, 35–57.

Zagorchev, I., and M. Ruseva (1993), Kriva Palanka and Kjustendil map sheets: Explanatory notes, Geological map of Bulgaria, scale 1:100,000, Bulg. Comm. of Geol., Sofia.

Zagorchev, I., and K. Sapundziev (1982), Deformation during the Early Alpine orogeny of the Poletintsi-Skrino fault zone. III. Ujno Allochthon (in Bulgarian), *Geotectonic Tectonophys. Geodyn.*, *14*, 3–31.

Zaun, P. E., and G. A. Wagner (1985), Fission-track stability in zircons under geological conditions, *Nucl. Tracks*, *10*, 303–307.

Zimmerman, J., Jr. (1972), Emplacement of the Vourinos ophiolitic complex, northern Greece, in *Studies in Earth and Space Sciences*, edited by R. Shagam et al., *Mem. Soc. Geol. Am.*, *132*, 225–239.

D. Bernoulli, J.-P. Burg, and D. Seward, Geology Institute, ETH Zurich and Zürich University, Sonneggstrasse 5, CH-8092 Zürich, Switzerland.

R. Handler, Bureau for Geology and Hydrology, Carl-Zuckmayer-Str. 1, A-5020 Salzburg, Austria.

Z. Ivanov, Faculty of Geology and Geography, University Kliment Ochridski, Boulevard Tsar Osvoboditel, 15, 1000 Sofia, Bulgaria.

A. Kounov, Institute of Geology and Palaeontology, Basel University, Bernoullistrasse, 32, CH-4056 Basel, Switzerland. (a.kounov@unibas.ch)